THE UNIVERSITY OF READING

Numerical Solution of Hyperbolic Systems of Conservation Laws with Source Terms - Part I

by

A.C. Lemos, M.J. Baines and N.K. Nichols

Numerical Analysis Report 1/2001

DEPARTMENT OF MATHEMATICS

Numerical solution of hyperbolic systems of conservation laws with source terms - Part I

A. C. Lemos[1] **, M. J. Baines and N. K. Nichols**

Numerical Analysis Report .../01

Department of Mathematics
The University of Reading
PO Box 220 Whiteknights
Reading Berkshire RG6 6AX
United Kingdom

March 13, 2001

[1]Supported by the grant PRAXIS XXI/BD/15905/98 from the *Subprograma Ciência e Tecnologia do 2° Quadro Comunitário de Apoio* and by the *Escola Superior de Tecnologia e Gestão* from the *Instituto Politécnico de Leiria*

Abstract

The water flow in an open channel can be described by the Saint-Venant equations which can be written as a system of hyperbolic conservation laws with source terms. In this report we study numerical schemes for the case of steady state flows in nonprismatic channels with rectangular cross-section and variable breadth function. The numerical schemes adopted are based on the Roe and Engquist-Osher schemes and have been constructed in two ways: a direct approach where the derivative of the flux function is discretised directly and an indirect approach where the chain rule is used to split the derivative of the flux function and the term due to variable breadth function is treated as a source term. In all cases the source terms are discretised pointwise (and centrally if they involve a derivative).

We show that the best numerical scheme in the direct approach is the Engquist-Osher scheme and that both the Engquist-Osher and the Roe schemes have good behaviour in the indirect approach. Overall the Engquist-Osher method seems to be the scheme behaving best in the two approaches.

Contents

Chapter 1

Introduction

One-dimensional systems of hyperbolic conservation laws with source terms can be written in the form

$$\mathbf{w}_t + \mathbf{F}(x, \mathbf{w})_x = \mathbf{D}(x, \mathbf{w}). \tag{1.1}$$

The function $\mathbf{F}$ is a *flux function*, the function $\mathbf{D}$ is a *source term* and $\mathbf{w}$ is the vector of conserved quantities. If $\mathbf{D}(x, \mathbf{w}) = \mathbf{0}$ then equations (1.1) are said to be in *conservative form.*

Particular cases are systems where the flux function $\mathbf{F}$ and the source function $\mathbf{D}$ depend only on $\mathbf{w}$

$$\mathbf{w}_t + \mathbf{F}(\mathbf{w})_x = \mathbf{D}(\mathbf{w}). \tag{1.2}$$

A practical application of systems of the form (1.1) is to the flow of water in a non-prismatic open channel with a variable bed. Another example is the quasi-one dimensional flow of a perfect compressible inviscid gas in pipes with constant or smoothly varying circular cross-section (see [4, 8]) or in a nozzle (see [1]). This flow is modelled by the Euler equations. Other applications are possible (see [24] for more details).

In the particular case we are interested in, the system of equations (1.1) describes the flow of water in an open channel of rectangular cross-section and variable bed and breadth functions (if the breadth function is constant, the function $\mathbf{F}$ depends only on $\mathbf{w}$ as in (1.2)) (see [18]).

In this case we have a system of two equations where the source terms involve the bed slope as well as the breadth function and its derivative. There is also an extra term in $\mathbf{D}$ if we take into account the bottom friction.

The discretisation of the source terms has been studied by many authors (see, e.g., [12, 9, 13, 7, 6, 16, 18, 25, 17, 21, 10, 4, 19], the work of [18, 25, 7] being particularly relevant for this work.

The source term can cause problems in accurately approximating (1.1), in particular if the source term is stiff (see [17]).

Some useful references on the numerical solution of hyperbolic systems of conservation laws are [15, 14, 11, 24].

In the next chapter the Saint-Venant equations describing water flow in an open channel are introduced as well as some of their properties. In chapter 3 we describe the numerical schemes used, based on the Engquist-Osher [5] and Roe [20] schemes. The numerical results obtained are discussed in Chapter 4. Finally, in Chapter 5, we present some general conclusions and discuss further work.

Chapter 2

The Saint-Venant equations

In this chapter the Saint-Venant equations are introduced and some of their properties are discussed with the main focus being the steady-state case.

Under the assumption of steady-state flow the Saint-Venant equations reduce to a single nonlinear ordinary differential equation describing the variation of the free surface.

In Section 2.1 we introduce the Saint-Venant equations and some notation. In Section 2.2 the particular case of a prismatic cross-section channel is studied and a rectangular cross-section channel will be assumed thereafter. The characteristic speeds are presented in Section 2.3. The steady-state case is the main focus in Section 2.4 and 2.5. The aim of Section 2.6 is to discuss ways to deal with the source terms.

2.1 The Saint-Venant equations for channels with variable breadth and rectangular cross-section

The one dimensional free surface water flow in a channel can be modelled by the Saint-Venant equations (see [3, 18]). These equations can be written as a system of equations of the form (1.1) with

$$\mathbf{w} = \begin{pmatrix} A \\ Q \end{pmatrix}, \quad \mathbf{F}(x, \mathbf{w}) = \begin{pmatrix} Q \\ \frac{Q^2}{A} + gI_1 \end{pmatrix}, \quad \mathbf{D}(x, \mathbf{w}) = \begin{pmatrix} 0 \\ gI_2 + gA(S_0 - S_f) \end{pmatrix}, \tag{2.1}$$

where

$$I_1 = \int_0^h (h - \eta)\sigma \, d\eta \tag{2.2}$$

and

$$I_2 = \int_0^h (h - \eta)\sigma_x \, d\eta. \tag{2.3}$$

For simplicity, the channel is assumed symmetric about the plane $y = 0$ (see Fig. 2.1 and Fig. 2.3). The notation used in (2.1) is the following (see also Fig. 2.2)

$x \in [0, L]$, L being the length of the channel

$h(x, t)$ is the depth, i.e. the level of the free surface above the bed level

$u(x, t)$ is the x-component of the fluid velocity

$A(x, t) = \int_0^h \sigma(x, \eta) \, d\eta$ is the wetted area

$Q(x, t)$ is the discharge, i.e. total volume of the flux through a given cross-section

$b(x)$ is the channel breadth

g is the acceleration due to gravity

$\sigma(x,t)$ is the width of channel as a function of both x and η

$\eta(x,t)$ is a coordinate which measures height relative to a fixed level

$z_b(x)$ is the height of the lowest point of the cross-section

$S_0 = -z_b'$ is the bed slope

S_f is the friction slope which models the effects of viscosity through friction with the solid boundaries.

In this model it is assumed that both σ and z_b are continuously differentiable functions and that $Q > 0$ everywhere (if $Q < 0$, just reverse the x direction to obtain $Q > 0$).

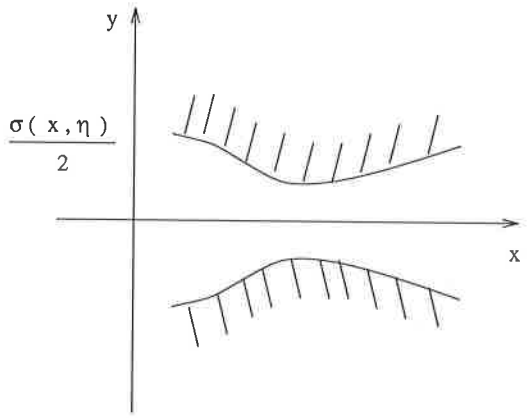

Figure 2.1: Horizontal cross section of a channel at height η

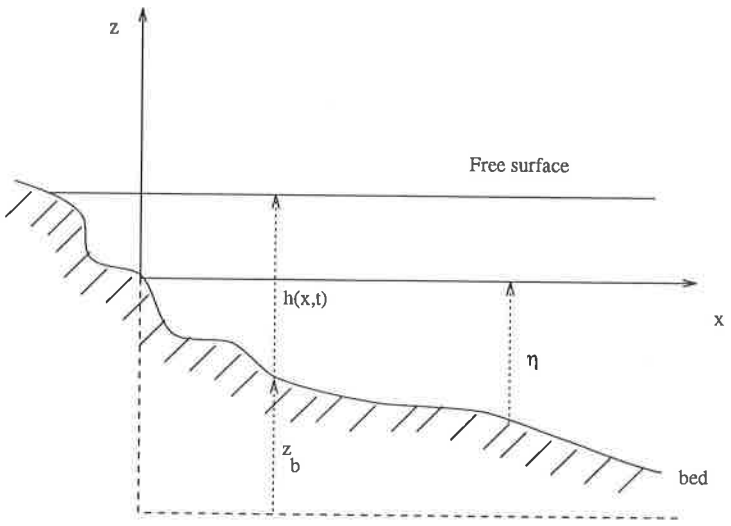

Figure 2.2: y-cross section showing bed and free surface

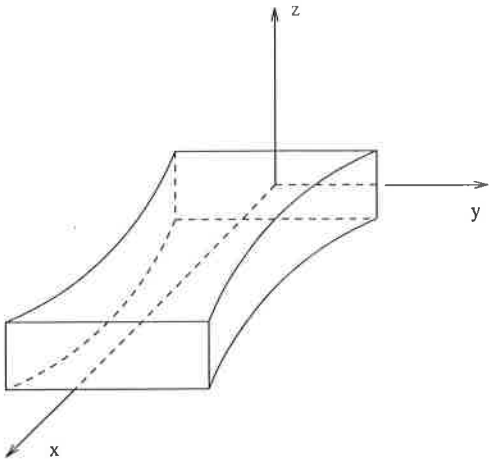

Figure 2.3: Sketch of a channel with rectangular x-cross section and variable breadth function (constant bed slope)

The quantity S_f is usually written (see [18]) in the form

$$S_f = \frac{Q|Q|}{K^2} \tag{2.4}$$

where P is the perimeter, K is the *conveyance* given by

$$K = \frac{A^{k_1}}{nP^{k_2}} \tag{2.5}$$

and n is a constant representing the roughness of the channel. The friction slope S_f can be expressed by using Chezy's or Manning's laws (see [3]). Here the Manning formulation for the friction slope S_f is adopted, i.e. $k_1 = 5/3$, $k_2 = 2/3$ and the *Manning coefficient*, n, is chosen to take the value 0.03.

In the following section the case of prismatic cross-section channels is studied and some new notation is introduced.

2.2 Prismatic cross-section channels

If the channel has prismatic cross-section but variable breadth, the function σ can be written as $\sigma = b(x) + 2hZ$ (see Fig. 2.4).

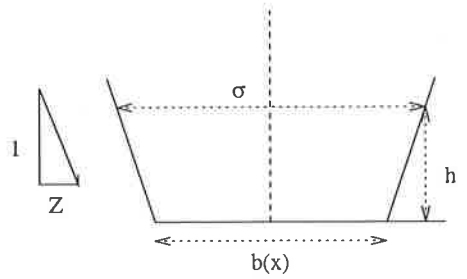

Figure 2.4: x-cross section showing a trapezoidal channel

We present a table, Table 2.1, with the expressions of some of the variables according to different types of prismatic cross-section and according to the breadth function being constant or variable.

Breadth variable Trapezoidal cross-section	Breadth variable Rectangular cross-section	Breadth constant Trapezoidal cross-section
$b(x) > 0,\ Z > 0$	$b(x) > 0,\ Z = 0$	$b(x) = B > 0,\ Z > 0$
$\sigma(x,h) = b(x) + 2hZ$	$\sigma(x,h) = b(x)$	$\sigma(h) = B + 2hZ$
$A(x,h) = h(b(x) + hZ)$	$A(x,h) = hb(x)$	$A(h) = h(B + hZ)$
$P(x,h) = b(x) + 2h\sqrt{1+Z^2}$	$P(x,h) = b(x) + 2h$	$P(h) = B + 2h\sqrt{1+Z^2}$
$I_1 = \frac{1}{2}h^2 b(x) + \frac{1}{3}Zh^3$	$I_1 = \frac{1}{2}h^2 b(x)$	$I_1 = \frac{1}{2}h^2 B + \frac{1}{3}Zh^3$
$I_2 = \frac{1}{2}h^2 b'(x)$	$I_2 = \frac{1}{2}h^2 b'(x)$	$I_2 = 0$

Table 2.1: Some formulas for the Saint-Venant equations (with and without breadth function being constant) corresponding to rectangular and trapezoidal cross-sections

The case where the breadth function is variable and the cross section is rectangular ($b(x)$ >0 and $z = 0$) is the one studied here.

2.3 Characteristic speeds

Actually the function $\mathbf{F}(x, \mathbf{w})$ in (2.1) can be thought of as a function of $b(x)$ and $\mathbf{w}$, $\overline{\mathbf{F}}(b(x), \mathbf{w})$. In the particular case of variable breadth function and rectangular cross section we have

$$\overline{\mathbf{F}}(b(x), \mathbf{w}) = \begin{pmatrix} Q \\ \frac{Q^2}{A} + \frac{1}{2}gAh \end{pmatrix} = \begin{pmatrix} Q \\ \frac{Q^2}{A} + \frac{1}{2}g\frac{A^2}{b(x)} \end{pmatrix}. \tag{2.6}$$

Hence

$$\frac{\partial \mathbf{F}}{\partial x} = \frac{\partial \overline{\mathbf{F}}}{\partial b}\frac{db}{dx} + \frac{\partial \overline{\mathbf{F}}}{\partial \mathbf{w}}\frac{\partial \mathbf{w}}{\partial x} \tag{2.7}$$

where

$$\frac{\partial \overline{\mathbf{F}}}{\partial b} = \begin{pmatrix} 0 \\ -\frac{1}{2}gh^2 \end{pmatrix} \tag{2.8}$$

and

$$\frac{\partial \overline{\mathbf{F}}}{\partial \mathbf{w}} = \mathbf{J} = \begin{pmatrix} 0 & 1 \\ gh - u^2 & 2u \end{pmatrix}. \tag{2.9}$$

The Jacobian matrix $\mathbf{J}$ has eigenvalues $\lambda_1 = u + c$, $\lambda_2 = u - c$, which give the characteristic speeds, (c is the *wave celerity* and is given by $c^2 = gA/b$ for a rectangular cross-section channel) and eigenvectors

$$\mathbf{r}_1 = \begin{pmatrix} 1 \\ u + c \end{pmatrix}, \qquad \mathbf{r}_2 = \begin{pmatrix} 1 \\ u - c \end{pmatrix}. \tag{2.10}$$

2.4 The Steady Problem

The steady flow equations can be obtained from the equations (1.1) by assuming no time dependence. In this case equations (1.1) reduce to

$$\begin{aligned} \frac{dQ}{dx} &= 0 \\ \frac{dF}{dx} &= D, \end{aligned} \tag{2.11}$$

with F and D being, respectively, the second components of $\mathbf{F}$ and $\mathbf{D}$. The first equation corresponds to a constant discharge and hence (2.11) can be written as a unique nonlinear ordinary differential equation of the form

$$\frac{dF(x,h)}{dx} = D(x,h), \tag{2.12}$$

or equivalently,

$$\frac{dh}{dx} = \frac{S_0 - S_f + \frac{Q^2}{gA^3}\int_0^h \sigma_x \, dx}{1 - F_r^2}. \tag{2.13}$$

As we can see, the denominator of equation (2.13) vanishes when

$$F_r = \sqrt{\frac{Q^2\sigma(x,h)}{gA^3}} = \frac{|u|}{c} = 1, \qquad (F_r = \textit{ Froude number}) \tag{2.14}$$

which corresponds to critical flow. The flow is called *supercritical* if $F_r > 1$ and *subcritical* if $F_r < 1$ (note that $\sigma(x,h) = b(x)$ in the case of a channel with rectangular cross-section).

Summarising, in the steady case, the Saint-Venant equations (1.1) reduce to a single equation of the form (2.12) with discharge Q constant, $F(x,h) = \frac{Q^2}{A} + gI_1$ and $D(x,h) = gI_2 + gA(S_0 - S_f)$.

2.5 Steady boundary conditions

Since the steady solution of the Saint-Venant equations is a particular example of the unsteady equation, the boundary condition requirements should be the same but obeying the rule of being constant in time.

With $Q > 0$, we have also $u > 0$ and consequently, $\lambda_1 > 0$ (see Section 2.3). Hence a variable has to be specified at inflow (for either supercritical or subcritical flow) and that variable should be Q which we know remains constant in the steady-sate case.

If the flow is supercritical at inflow ($\lambda_2 > 0$) we have to specify another variable at inflow, and we choose the depth h. No variables have to be specified for supercritical outflow.

If the flow is subcritical at outflow ($\lambda_2 < 0$) we have to specify another variable at outflow, and we choose the depth h. No additional variable has to be specified for subcritical inflow.

2.6 Source terms

One possible approach to deal with the source terms is to split the inhomogeneous problem into an advection problem (homogeneous) and a source problem (ordinary differential equation) and then treat the resulting problems independently (see e.g. [24]). This is not the approach adopted here. Instead we use numerical schemes based in the Roe [20] and Engquist-Osher [5] schemes to solve the entire equation (2.12) numerically.

Roe's scheme has been used by many authors to solve systems of the form (1.2) numerically (e.g. [2, 6, 18, 19, 20]) and also of the form (1.1) (e.g. [7, 13, 18, 25]). These works point towards a discretisation of the source terms coupled with the way the derivative of the flux function is discretised.

The use of the Engquist-Osher scheme [5] for problems of the form (1.1), even in the steady-state case, has not been so thoroughly studied. Special mention to the work of MacDonald [18] is due, which was fundamental to our study. Some of the ideas presented

in [18] are developed further in the present report. Although MacDonald used both the Engquist-Osher and the Roe schemes to solve problems of the form (1.2) and (1.1) in the steady-sate case, some questions remain unanswered. For example, which is the best discretisation of the source terms, particularly if the Roe method is used.

In this report we did not aim to do an upwind discretisation of the source terms. Nevertheless we present some results of an upwind approach depending strongly on special knowledge of the test problems and hence of not very practical use otherwise. The upwind discretisation of the source terms will be the subject of a future report. Hence, in the present work, the source terms were discretised pointwise if we were using the Engquist-Osher scheme and averaged between neighbouring grid points if we were using the Roe scheme. Some of the numerical schemes involve the need to discretise a source term which is a derivative, as we will see in the next chapter. In this case a centred approximation (or a centred approximation at the half-point) is taken to approximate the derivative term.

In the next chapter the numerical schemes used to approximate (2.12) are described. The work of MacDonald [18] is central to this report and to the next chapter in particular. In fact we followed some of his ideas and extended others and used some of the test problems in [18] to test our algorithms.

Chapter 3

Discretisation

A uniform grid was used. For a channel of length L ($x \in [0, L]$), we have $x_i = ih$, $i = 0, 1, \ldots, N$ with a spacing $h = L/N$ ($N \in \mathbb{N}$).

Following the work of MacDonald [18] the numerical solution to (2.12) was sought by using a finite difference discretisation combined with a time stepping iteration. Hence if $\mathcal{T}_j$ represents the finite difference operator approximating the differential operator

$$\mathcal{T}h = \frac{dF(x,h)}{dx} - D(x,h), \tag{3.1}$$

the time-stepping iteration has the form

$$\frac{h_j^{n+1} - h_j^n}{\Delta t} + \mathcal{T}_j h^n = 0 \qquad\qquad n = 0, 1, \ldots \tag{3.2}$$

where the superscript notation indicates the iteration and the subscript notation indicates the grid point. So h_j^n represents an approximation to $h(x_j)$ at the iteration n. The initial approximation h^0 was taken to be, as suggested in [18], the linear depth profile joining the values of the boundary conditions (when provided) or/and the value of the critical depth function at the endpoint needed. (Note that for the case of a rectangular cross-section it is possible to obtain the function $h_c(x)$ explicitly).

The discretisation of the derivative of the flux function, $\frac{dF(x,h)}{dx}$,was considered in two ways. One way was to take into account the explicit dependence of the derivative of F on x directly in the discretisation. This approach was taken by MacDonald [18] when using an Engquist-Osher method to solve (2.12). The other way was to split the derivative of F by the chain rule and to keep the terms depending on h (x fixed) on the left-hand side, treating the other terms (due to variable breadth function) depending on x (h fixed), as source terms. This idea was also explored in the work of [7, 25, 13] for problems of the form (1.1).

A suitable discretisation of the source terms was sought for both ways adopted to discretise the derivative of the flux function.

Schemes based on both Engquist-Osher [5] and Roe [20] schemes were used.

In the following we describe in more detail how this discretisation was implemented.

3.1 Direct discretisation of $\frac{dF(x,h)}{dx}$

In order to model numerically the dependence of F on x directly we allowed the numerical flux function to also depend on x. (We shall use the notion of numerical flux function even

for these inhomogeneous problems). A possible first-order approximation of $(F(x,h))_x$ in the interval (x_j, x_{j+1}) is given by

$$\frac{d}{dx}F(x,h) \approx \frac{g(x_{j+q}, h_{j+1}, h_j) - g(x_{j+q-1}, h_j, h_{j-1})}{\Delta x}, \tag{3.3}$$

for any real q (see [18]), where

$$x_{j+q} = (j+q)\Delta x \tag{3.4}$$

and g is consistent with F, i.e.

$$g(x,h,h) \equiv F(x,h). \tag{3.5}$$

A Godunov-type interpretation (see [23]) of $g_{j+\frac{1}{2}}$ as the time average across the cell interface at $x = x_{j+\frac{1}{2}}$, points to a choice of $q = \frac{1}{2}$. Nevertheless the cases $q = 0, 1$ were also studied.

The choice of the parameter q was thought of in two ways, firstly, fixing the parameter q ($q = 0, 1, \frac{1}{2}$) from the start and secondly, changing it according to 'the wind' ($q = 0$ or $q = 1$). The first approach is used in schemes 1 and 2 below and the second approach in schemes 3 and 4.

Scheme 1 is obtained from the Engquist-Osher scheme [5] by adding the argument x to any evaluations of the function F and its derivatives (see [18]). The corresponding numerical flux function is

$$g_1(x,u,v) = F^-(x,u) + F^+(x,v) + F(x,a) \tag{3.6}$$

where

$$\begin{aligned} F^-(x,u) &= \int_a^u \min_s\{F_s(x,s), 0\}\, ds \\ F^+(x,u) &= \int_a^u \max_s\{F_s(x,s), 0\}\, ds \end{aligned} \tag{3.7}$$

and $a > 0$ is arbitrary.

Scheme 1 was used in [18] and there a comparison between the three choices of the parameter q mentioned above ($q = 0, 1, 0.5$) can be found. Hence here we just present some results with the choice $q = 0.5$ because this seems to give a good behaviour for all the test problems.

Scheme 2, based on the Roe scheme [20], is constructed in a similar way, by adding the argument x to any evaluations of the function F or its derivatives. In this way we obtain a Roe based scheme with the numerical flux function given by

$$g_2(x_k, h_R, h_L) = \frac{1}{2}\left[F(x_k, h_R) + F(x_k, h_L) - |s_{LR}|(h_R - h_L)\right] \tag{3.8}$$

with

$$s_{LR} = \begin{cases} \frac{F(x_k,h_R) - F(x_k,h_L)}{h_R - h_L} & h_R \neq h_L \\ \\ F_h(x_k, h_L) & h_R = h_L \end{cases} \tag{3.9}$$

where x_L and x_R represent two neighbouring grid points and the point x_k was chosen to be either x_L or x_R or the midpoint of the interval $[x_L, x_R]$, $\frac{x_L + x_R}{2}$ (the numerical results presented correspond to this last choice of x_k).

The other idea mentioned was to think of the parameter q varying according to 'the wind'. The numerical results used for this case were obtained by using two schemes, one based on the Engquist-Osher scheme (scheme 3) and the other based on the Roe scheme (scheme 4). The idea in scheme 3 is to build a scheme similar to scheme 1 but where the parameter q is allowed to vary taking the values 0 or 1. So if the flow is entirely subcritical, $q = 1$ and if the flow is entirely supercritical $q = 0$. If in the interval considered the flow changes from subcritical to supercritical (resp. supercritical to subcritical), the parameter q will change from 1 to 0 (resp. from 0 to 1). The scheme will be explained in more detail in Section 3.4. Scheme 4, based on the Roe scheme, was constructed in a similar way and for the interval $[x_L, x_R]$ can be written with the help of a 'numerical flux function' given by

$$g_4(x_R, x_L, h_R, h_L) = \frac{1}{2}[F(x_L, h_L) + F(x_R, h_R) - |s_{LR}|(h_R - h_L)] \tag{3.10}$$

with

$$s_{LR} = \begin{cases} \frac{F(x_R,h_R)-F(x_L,h_L)}{h_R-h_L} & h_L \neq h_R \\ \\ F_h(x_L, h_L) & h_L = h_R. \end{cases} \tag{3.11}$$

Actually, another scheme differing from scheme 1 only in the way the decision is made, was built. The decision was taken to be the one in scheme 3 and it will be explained in more detail in Section 3.4. The results were similar to the ones of scheme 1 and therefore are not shown in the report.

3.2 Indirect discretisation of $\frac{dF(x,h)}{dx}$

Since by the chain rule the left-hand side of (2.12) can be written as

$$\frac{d}{dx}F(x,h) = \frac{\partial F}{\partial h}\frac{dh}{dx} + \frac{\partial F}{\partial b}\frac{db}{dx} \tag{3.12}$$

we can think of treating the term $\frac{\partial F}{\partial b}\frac{db}{dx}$ as a source term. This approach is not new when applied to a Roe-based scheme (see, e.g [18]) but it appears to be new for the Engquist-Osher scheme. (Generally the Roe scheme has been used in this way to solve the more general system of equations (1.1).)

In part 2 of this report the idea of discretising the source term according to the way the left-hand side is discretised it will be taken in account.

In this way we can construct the following finite difference approximation of left-hand side,

$$\frac{\partial F}{\partial h}\frac{dh}{dx} \approx \frac{g(x_k, h_{j+1}, h_j) - g(x_k, h_j, h_{j-1})}{\Delta x}, \tag{3.13}$$

where x_k is fixed. In scheme 5 we took $x_k = x_j$ (an Engquist-Osher based scheme) and $x_k = \frac{x_L+x_R}{2}$ for a Roe-based scheme, scheme 6. Scheme 5 is then built by using (3.13) together with the numerical flux function (3.6). Similarly, scheme 6 is built by using (3.13) together with the choice of numerical flux function given by (3.8).

3.3 Treatment of source terms

In the direct approach (see Section 3.1) the source term $D(x,h)$ has the form

$$D(x,h) = gI_2 + gA(S_0 - S_f) \tag{3.14}$$

where I_2 depends on both $b'(x)$ and h, S_0 is known exactly (from the way the test problem is given - see Section 4.1 for more details) and S_f is given by (2.4) and depends on both x and h.

In the indirect approach the source term has an added term which is the one corresponding to the part of the derivative $F(x,h)_x$ which is put on the right-hand side (see section 3.2). Let us call it $d(x,h)$. So the source term in this indirect case is

$$d(x,h) = D(x,h) - \frac{\partial F}{\partial b}\frac{db}{dx}. \tag{3.15}$$

Actually, expression (3.15) can be written in the form

$$d(x,h) = gI_2 + gA(S_0 - S_f) + \frac{Q^2}{A^2}hb'(x) - gI_2 = gA(S_0 - S_f) + \frac{Q^2}{A^2}hb'(x) \tag{3.16}$$

since gI_2 cancels.

In our test problems the source term (3.15) was not discretised globally but each term separately, i.e. $D(x,h)$ and $\frac{\partial F}{\partial b}\frac{db}{dx}$. In schemes 1, 3 and 5 we used a pointwise discretisation of $D(x,h)$, i.e.

$$D(x,h) \approx D(x_i,h_i), \tag{3.17}$$

whereas for schemes 2,4 and 6 we used an average between neighbouring grid points, i.e.

$$D(x,h) \approx \frac{D(x_L,h_L) + D(x_R,h_R)}{2}. \tag{3.18}$$

An upwind approach is also possible in the way described in [18] or some decomposed approaches for the full system as studied by [6, 13, 25, 8, 22]. In the latter case the source terms are approximated by a linear combination of the eigenvectors of a Roe matrix.

For the indirect schemes 5 and 6 it remains to work out a way to discretise the term $\frac{\partial F}{\partial x}$ when treated as a source term. We chose to approximate this source term with the derivative by a centred discretisation or a centred discretisation at the half-point.

3.4 Numerical schemes described in more detail

Here we describe in more detail the numerical schemes used.

The algorithms for the schemes 1,3 and 5 were implemented by using the numerical flux functions g_1 and g_3 as described in sections 3.1 and 3.2. The algorithms for the schemes 2, 4 and 6 were implemented in a different way, without the direct use of the numerical flux functions g_2, g_4, since that is more suitable for computational purposes. In this section we describe the algorithms used in more detail.

For scheme 1, supposing that there is a unique critical depth at each x cross-section $h_c(x)$ and because F is convex, we have

$$\begin{aligned} h_j, h_{j+1} < h_c(x_{j+q}) &\Rightarrow g(x_{j+q}, h_{j+1}, h_j) = F(x_{j+q}, h_{j+1}) \\ h_j, h_{j+1} > h_c(x_{j+q}) &\Rightarrow g(x_{j+q}, h_{j+1}, h_j) = F(x_{j+q}, h_j). \end{aligned} \tag{3.19}$$

But the cases of $h_j < h_c(x_{j+q}) < h_{j+1}$ and $h_{j+1} < h_c(x_{j+q}) < h_j$ have to be analysed as well. All the possible cases are taken in account if we rewrite (3.6) in the form

$$g_1(x_{j+q}, h_{j+1}, h_j) = \begin{cases} F(x_{j+q}, h_{j+1}) & h_{j+1}, h_j < h_c(x_{j+q}) \\ F(x_{j+q}, h_j) & h_{j+1}, h_j > h_c(x_{j+q}) \\ F(x_{j+q}, h_{j+1}) + F(x_{j+q}, h_j) - F(x_{j+q}, h_c(x_{j+q})) & h_j > h_c(x_{j+q}) > h_{j+1} \\ F(x_{j+q}, h_c(x_{j+q})) & h_j < h_c(x_{j+q}) < h_{j+1} \end{cases} \tag{3.20}$$

For scheme 3 the numerical flux function can be thought of as depending on two grid points, instead of one. The two grid points adopted are the endpoints of the interface. So the numerical flux for this scheme can be written as

$$g_3(x_{j+1}, x_j, h_{j+1}, h_j) = \begin{cases} F(x_{j+1}, h_{j+1}) & h_{j+1} < h_c(x_{j+1}) \text{ and } h_j < h_c(x_j) \\ F(x_j, h_j) & h_{j+1} > h_c(x_{j+1}) \text{ and } h_j > h_c(x_j) \\ F(x_{j+1}, h_{j+1}) + F(x_j, h_j) - F(x_j, h_c(x_j)) & \\ & h_{j+1} < h_c(x_{j+1}) \text{ and } h_j > h_c(x_j) \\ F(x_j, h_c(x_j)) & h_{j+1} > h_c(x_{j+1}) \text{ and } h_j < h_c(x_j). \end{cases} \tag{3.21}$$

The Roe-based schemes 2, 4 and 6 were implemented in the following way:

1. the values of s_{LR} were computed for every interval of the form $[x_L, x_R]$ and stored in an array
2. for each interval:
   (a) we compute the value of ΔF, that is,

$$\Delta F = F(x_k, h_R) - F(x_k, h_L) \tag{3.22}$$

   for schemes 2 and 6 and

$$\Delta F = F(x_R, h_R) - F(x_L, h_L) \tag{3.23}$$

   for scheme4;

   (b) we check the sign of s_{LR} to make the decision whether to update either h_L or h_R. Hence we have

   if $s_{LR} < 0$ then h_L is updated according to

$$h_L^{n+1} = h_L^n - \Delta t \Delta F / \Delta x \tag{3.24}$$

   if $s_{LR} > 0$ then h_R is updated according to

$$h_R^{n+1} = h_R^n - \Delta t \Delta F / \Delta x \tag{3.25}$$

3. for each interval the source terms are added to the updated variables
4. overwrite the values at endpoints with analytical boundary conditions if necessary.

Note that if an upwind approach were to be used the sign of s_{LR} also decides how to take in account the source term.

Since schemes 5 and 6 are similar to schemes 1 and 2 (with the numerical flux function computed at a fixed grid point) we will not explain them in more detail.

A different version of scheme 1 was also tried where we took the values of F as in scheme 1 but the decison was taken from scheme 3 instead. Since the results were very similar to scheme 1 we do not present them here.

Chapter 4

Numerical results

4.1 Test problems

The test problems were chosen from the ones presented in [18] such that different types of flow (inclusive of hydraulic jumps) are illustrated. These test problems are constructed in such a way that an analytical solution for the full steady Saint-Venant equations is known. The principle is that if a particular depth profile h is known, it is possible to compute (analytically) the bed slope S_0 that makes this profile an actual solution of the steady equation (see [18] for more details).

The four test problems chosen illustrate different flow features and correspond to the flux of a flow in an open channel of rectangular cross-section and with variable breadth function given by

$$b(x) = 10 - 5\exp\left\{-10\left(\frac{x}{200} - \frac{1}{2}\right)^2\right\}. \tag{4.1}$$

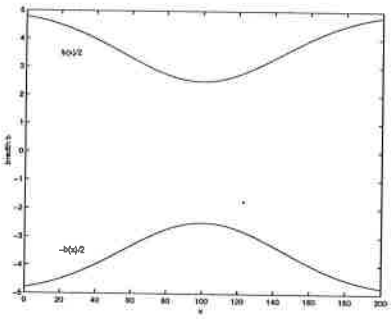

Figure 4.1: Graph of the horizontal cross-section of the channel

Manning's friction law was used with coefficient $n = 0.03$. The details of the test problem are given in tables 4.1 and 4.2.

The test problems were chosen from the ones given in [18] by MacDonald (test problems 9-12 in Appendix B) and correspond to different types of flow. The boundary conditions needed (see section 2.5) are given in table 4.2. Other boundary conditions (if needed) are taken as the values of the critical depth function h_c at the corresponding endpoints, as suggested by MacDonald [18].

The depth profile in test problem 1 is subcritical whereas in test problem 2 it is entirely supercritical. In test problem 3 the flow is subcritical until approximately one third of the length of the channel and then changes smoothly to supercritical. In test problem 4, a

Prob.	Type of flow	Analytical depth profile $\hat{h}$
1	Subcritical	$\hat{h}(x) = 0.9 + 0.3\exp\left(-20\left(\frac{x}{200} - \frac{1}{2}\right)^2\right)$
2	Supercritical	$\hat{h}(x) = 0.5 + 0.5\exp\left(-20\left(\frac{x}{200} - \frac{1}{2}\right)^2\right)$
3	Smooth transition	$\hat{h}(x) = 1.0 - 0.3\tanh\left(4\left(\frac{x}{200} - \frac{1}{3}\right)\right)$
4	hydraulic jump	$\hat{h}(x) = \begin{cases} 0.7 + 0.3\exp\left(\frac{x}{200} - 1\right) & x \leq 120 \\ exp(-0.1(x-120))\sum_{i=0}^{2} k_i \left(\frac{x-120}{200-120}\right)^i + \phi(x) & x > 120 \end{cases}$ where $k_0 = -.274406$, $k_1 = -.948343$ and $k_2 = 4.89461$ $\phi(x) = 1.5exp\left(0.1\left(\frac{x}{200} - 1\right)\right)$

Table 4.1: Test problem details: type of flow and analytical solution

Prob.	L/m	$Q/(m^3s^{-1})$	h_{in}/m	h_{out}/m
1	200	20		0.902921
2	200	20	0.503369	
3	200	20		
4	200	20	0.7	1.49924

Table 4.2: Test problem details: length of channel, discharge and boundary conditions

hydraulic jump occurs at $x = 120$m and the depth profile jumps there from supercritical to subcritical.

4.2 Results and discussion

We have considered two different measures of accuracy (L_2 norm) according to the type of scheme used. In schemes 1, 3 and 5 the criterion of convergence for the iterative method was

$$\sqrt{\frac{1}{N-1}\sum_{j=1}^{N-1}\left(\frac{h_j^{n+1} - h_j^n}{\Delta t}\right)^2} < TOL \tag{4.2}$$

and for schemes schemes 2, 4 and 6 the criterion of convergence for the iterative method was

$$\sqrt{\frac{1}{N+1}\sum_{j=0}^{N}\left(\frac{h_j^{n+1} - h_j^n}{\Delta t}\right)^2} < TOL. \tag{4.3}$$

Actually, we used a relative type of error measure corresponding to (4.2) and (4.3). For almost all the schemes, $TOL = 10^{-8}$ with the exceptions of scheme 3 where, for test problem 1 ($n = 10$ and $n = 20$), TOL had to be set higher, 10^{-4}. The numerical results of scheme 4 have an oscillatory behaviour and do not seem to converge whatever the TOL and Δt chosen. Hence no numerical results for that scheme will be presented here.

The approximate solutions obtained from schemes 1-3,5-6, to each test problem, are shown in Figures 4.2-4.10. It can be seen from the graphs that overall the approximate solution obtained from Engquist-Osher schemes (schemes 1, 3 and 5) is the most accurate, followed by scheme 6. In fact, the smallest L_2 error (for $N = 10, 20, 40, 80, 160$) is obtained:

in test problem 1 by scheme 1; in test problem 2 by scheme 3; in test problems 3-4 by scheme 5 (centred).

As expected, when N increases, the centred discretisation and the centred discretisation at half-point (schemes 5 and 6) yield a similar error (see Figures 4.21-4.28). The only case where an upwind discretisation (schemes 5 and 6) provides a more accurate solution than the centred discretisation is for problem 2 when using scheme 6 (see Figures 4.21, 4.23, 4.25 and 4.27 and also 4.18 and 4.19).

The idea in scheme 3 to change the parameter q in scheme 1 (as explained in section 3.1) does not seem to provide better results than the ones obtained through scheme 1 (see Figures 4.21-4.28).

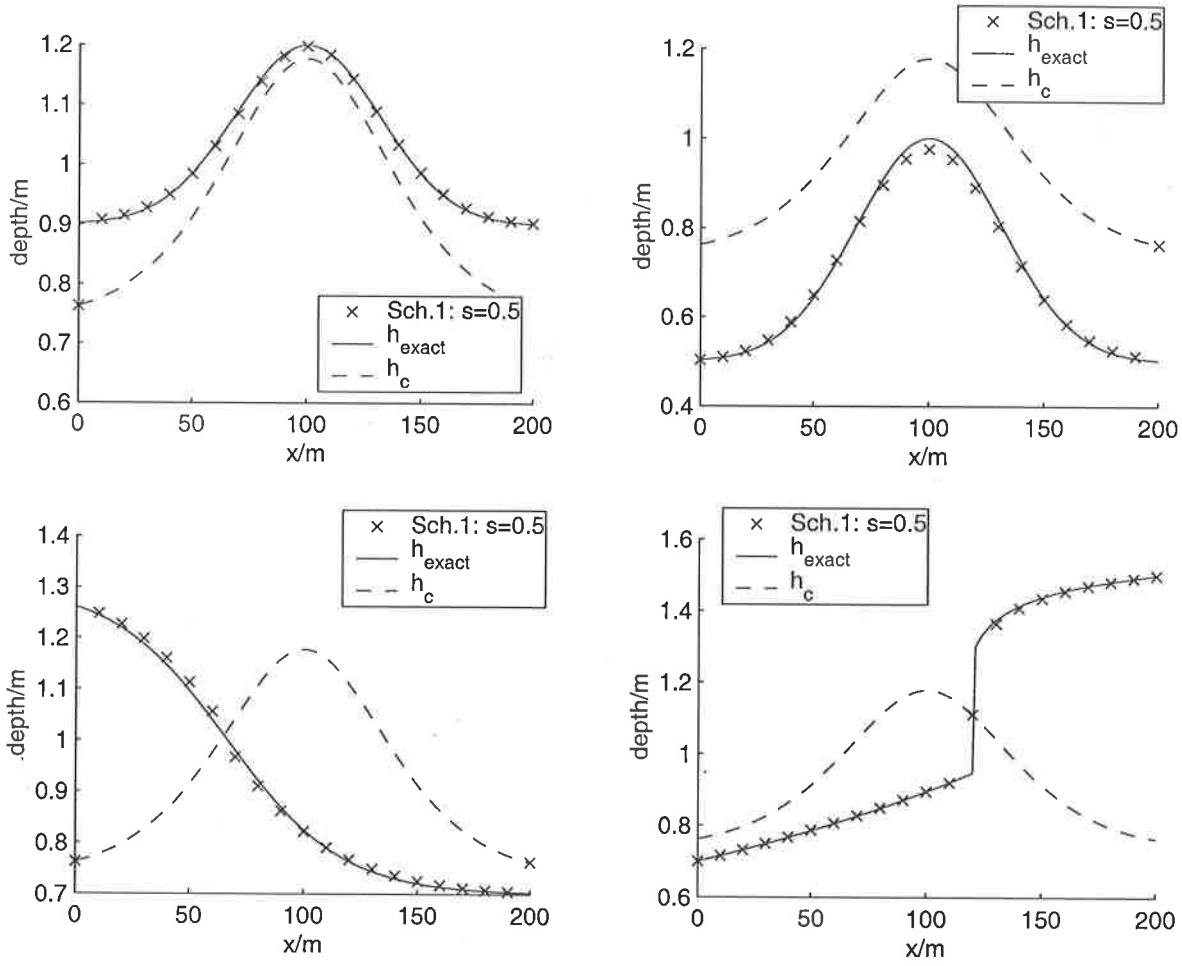

Figure 4.2: Scheme 1 for problems 1-4 ($\Delta x = 10$)

As we can see from Figure 4.3, scheme 2 generates a numerical solution that is not very accurate. In particular, for test problems 1 and 2 the numerical results are shifted to the right of the true solution and in test problem 3 the numerical solution forms a bump on the region of supercritical flow.

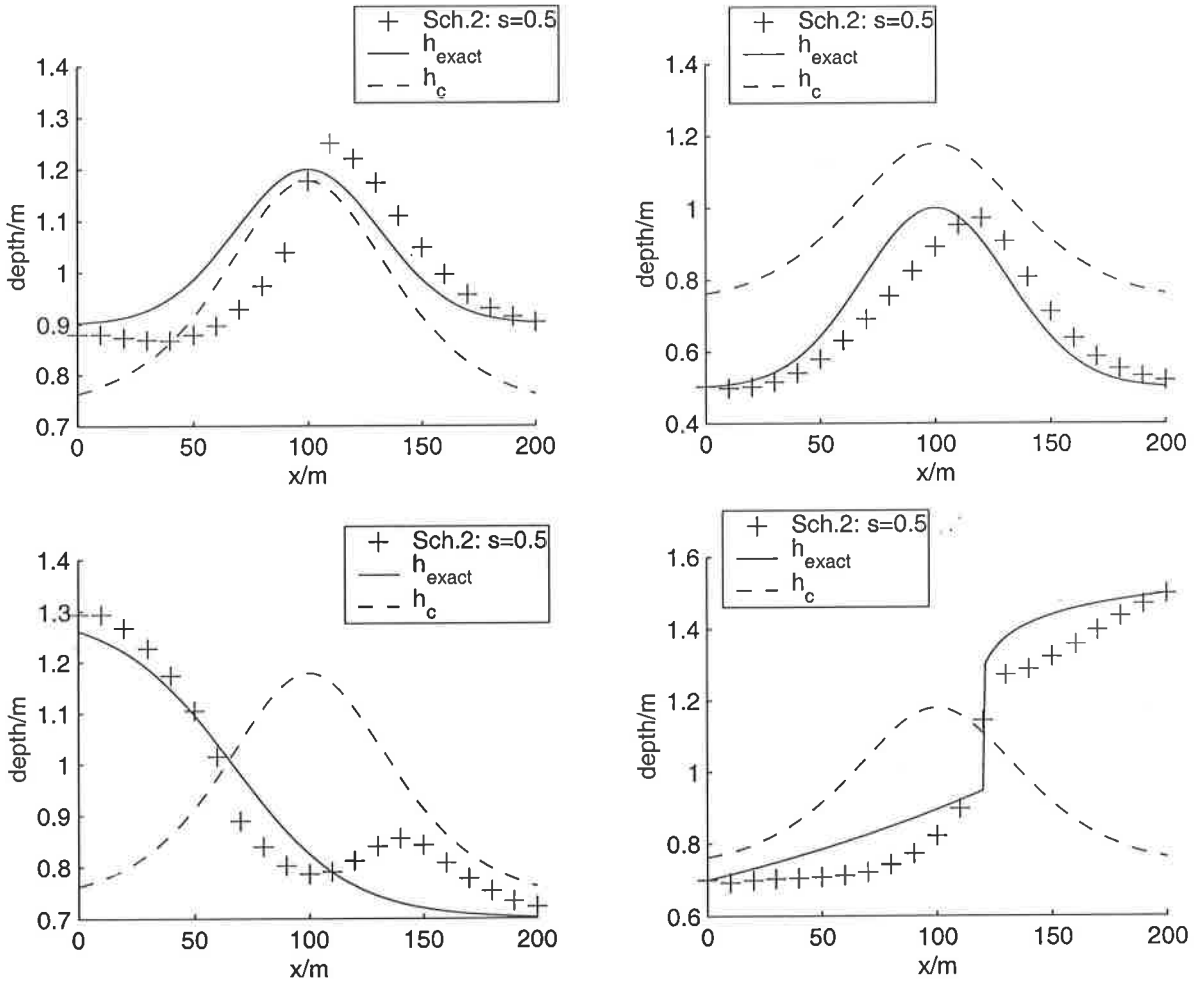

Figure 4.3: Scheme 2 for problems 1-4 ($\Delta x = 10$)

As we can see from Figure 4.4, scheme 3 seems to provide an accurate solution to all test problems. Moreover, from Figure 4.23 we can see that, for test problem 2, the results from scheme 3 have the smallest L_2 error.

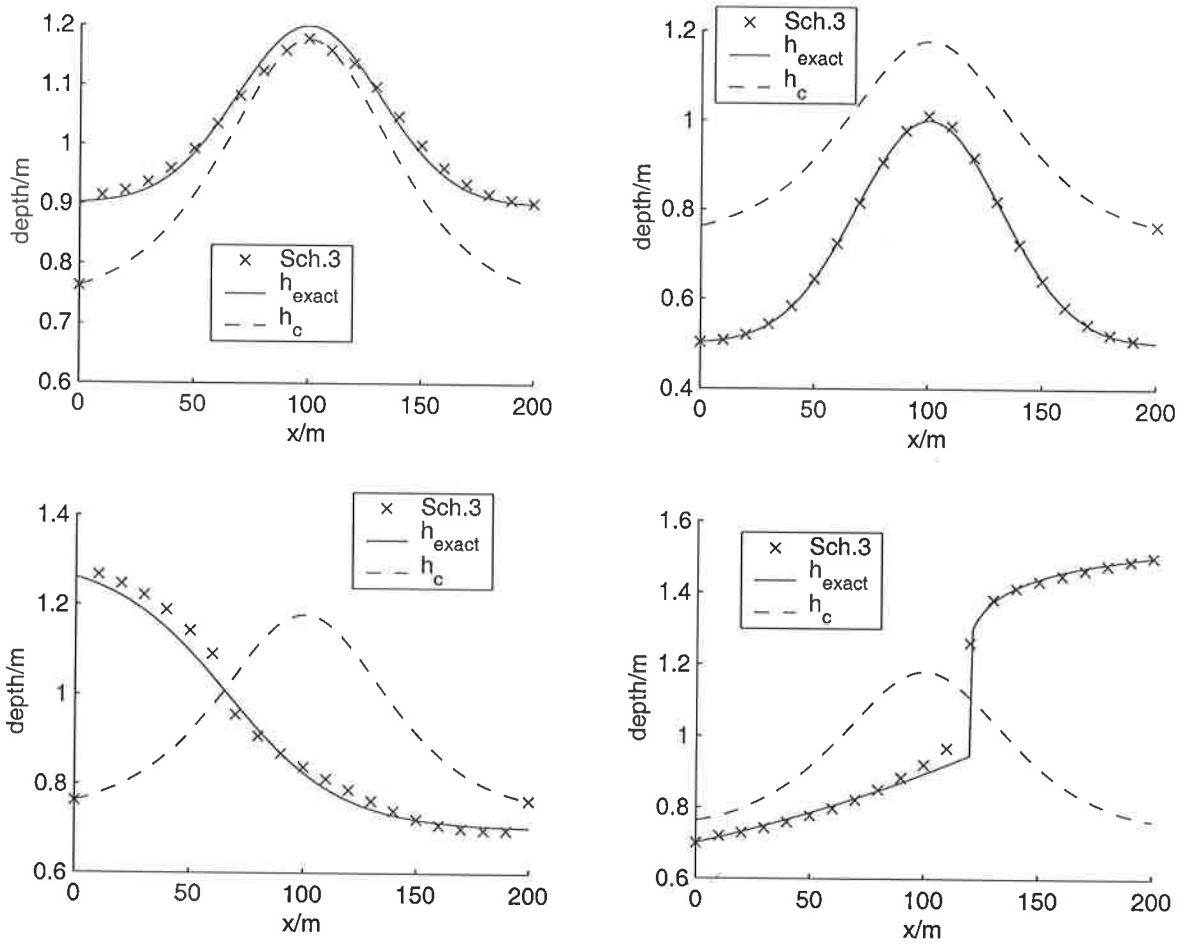

Figure 4.4: Scheme 3 for problems 1-4 ($\Delta x = 10$)

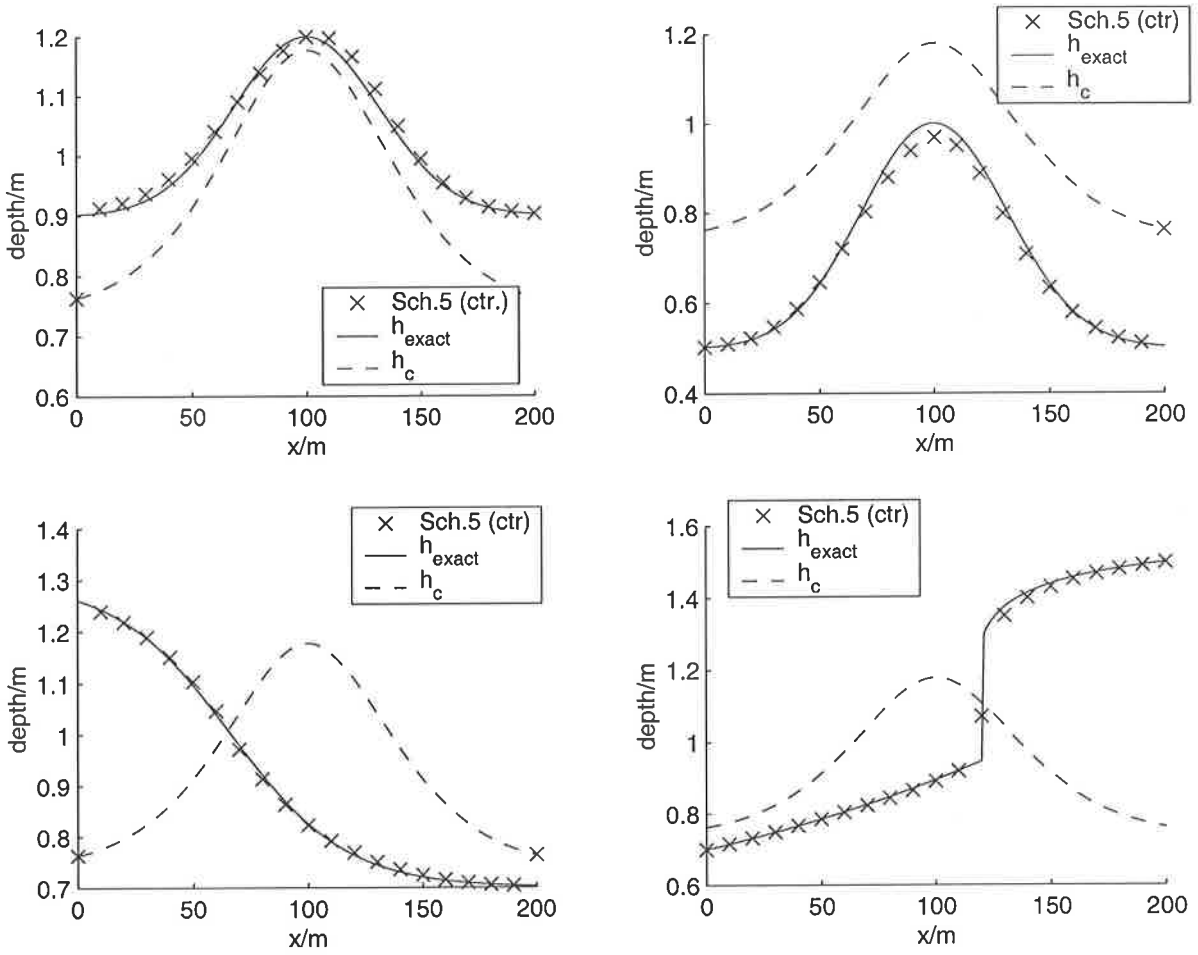

Figure 4.5: Scheme 5 (ctr.) for problems 1-4 ($\Delta x = 10$)

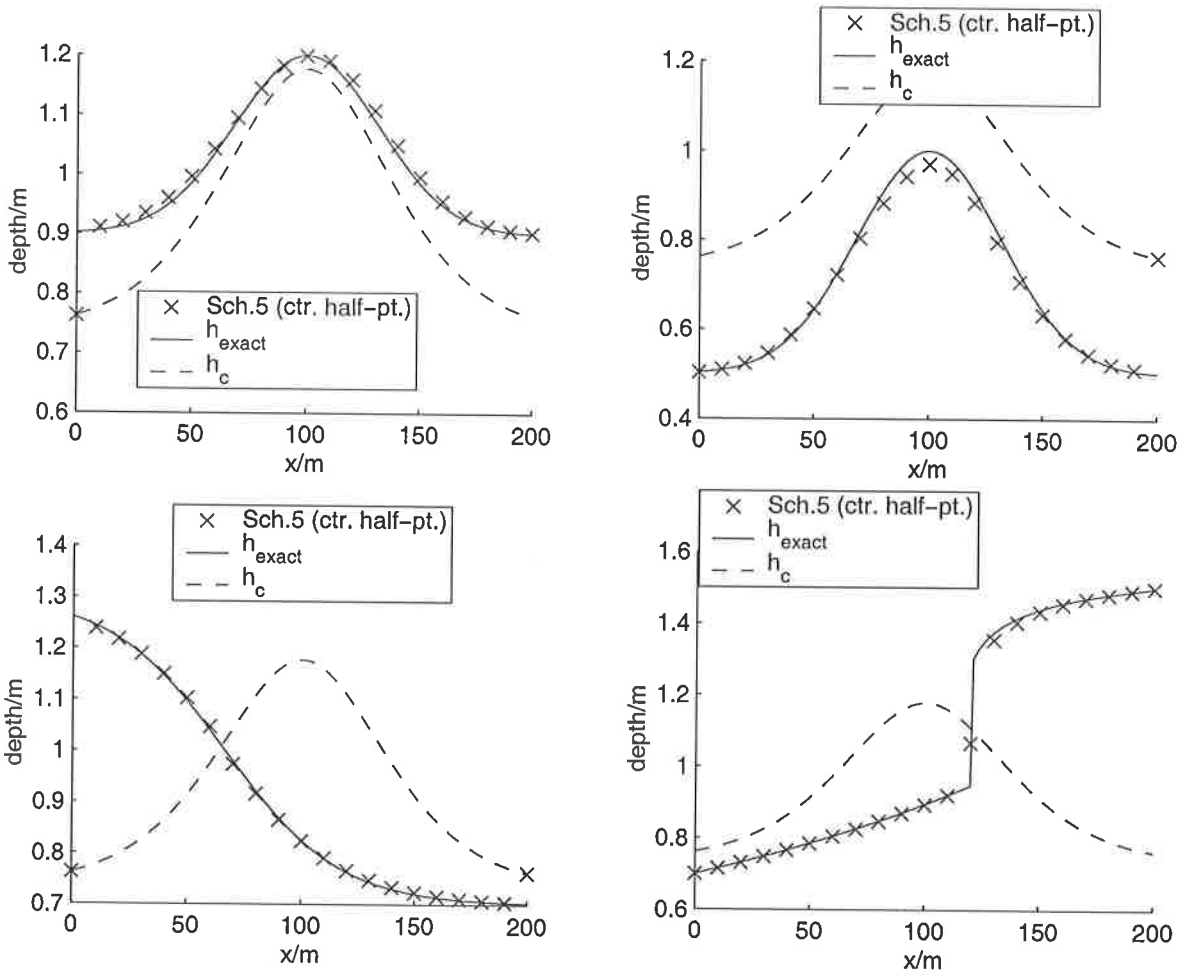

Figure 4.6: Scheme 5 (ctr. half-pt.) for problems 1-4 ($\Delta x = 10$)

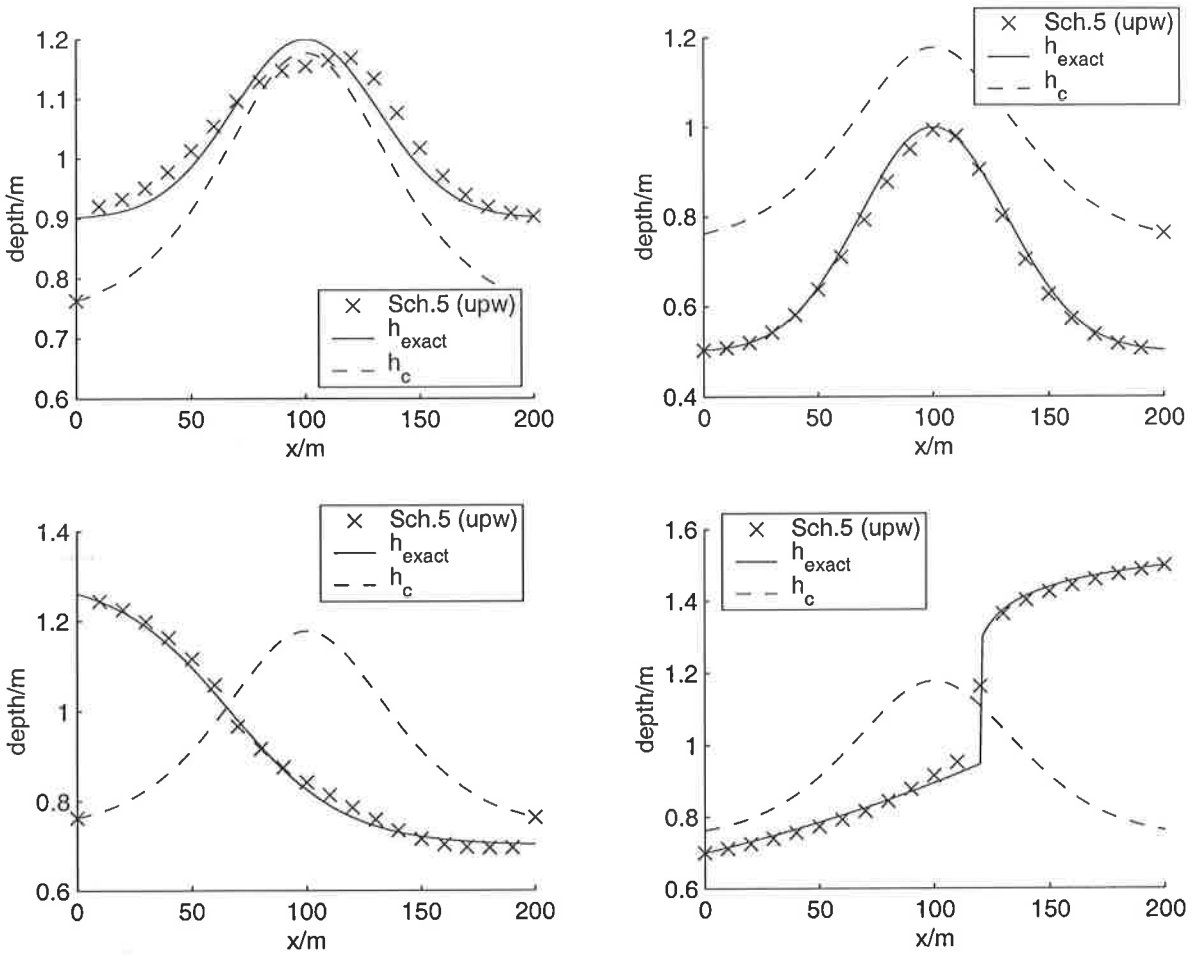

Figure 4.7: Scheme 5 (upw) for problems 1-4 ($\Delta x = 10$)

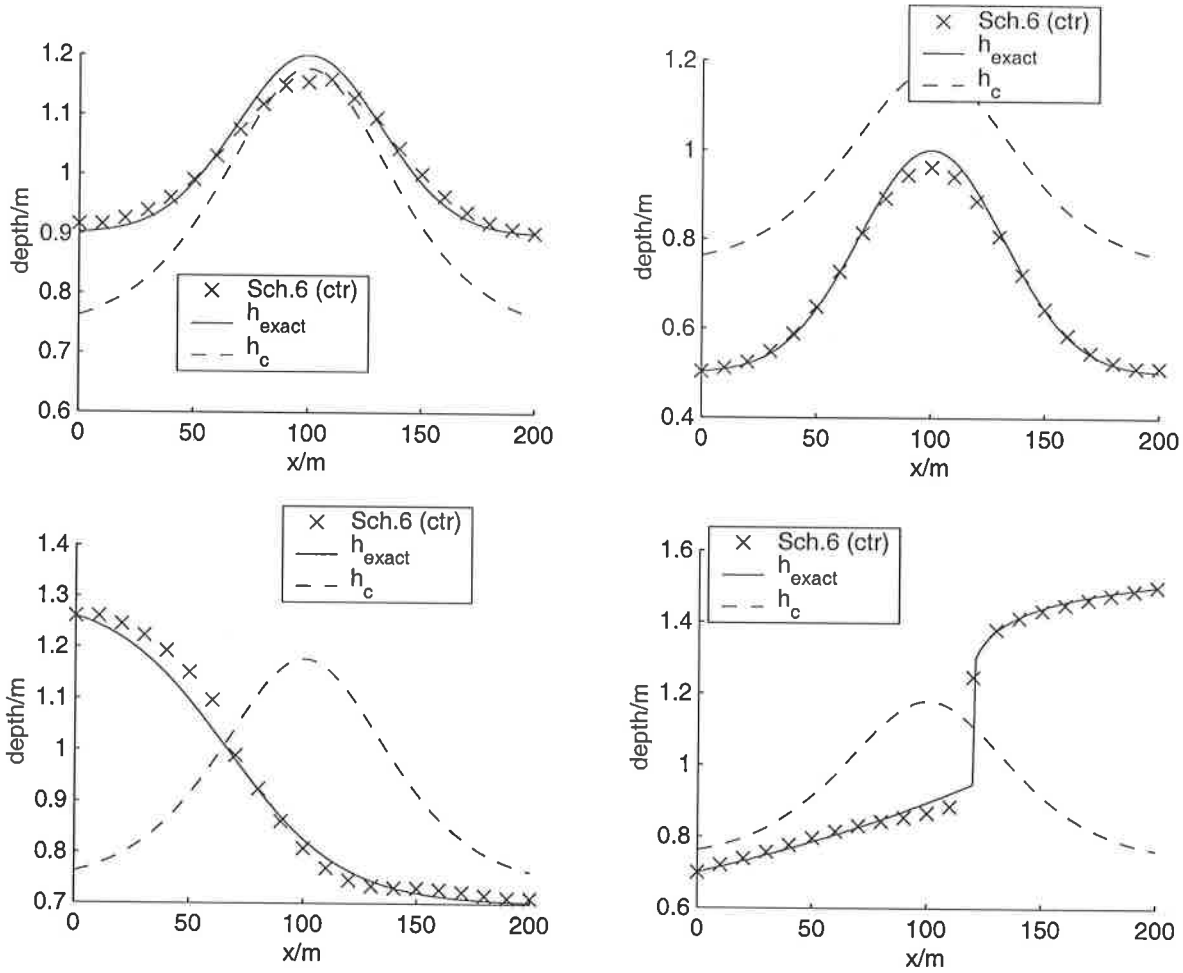

Figure 4.8: Scheme 6 (ctr.) for problems 1-4 ($\Delta x = 10$)

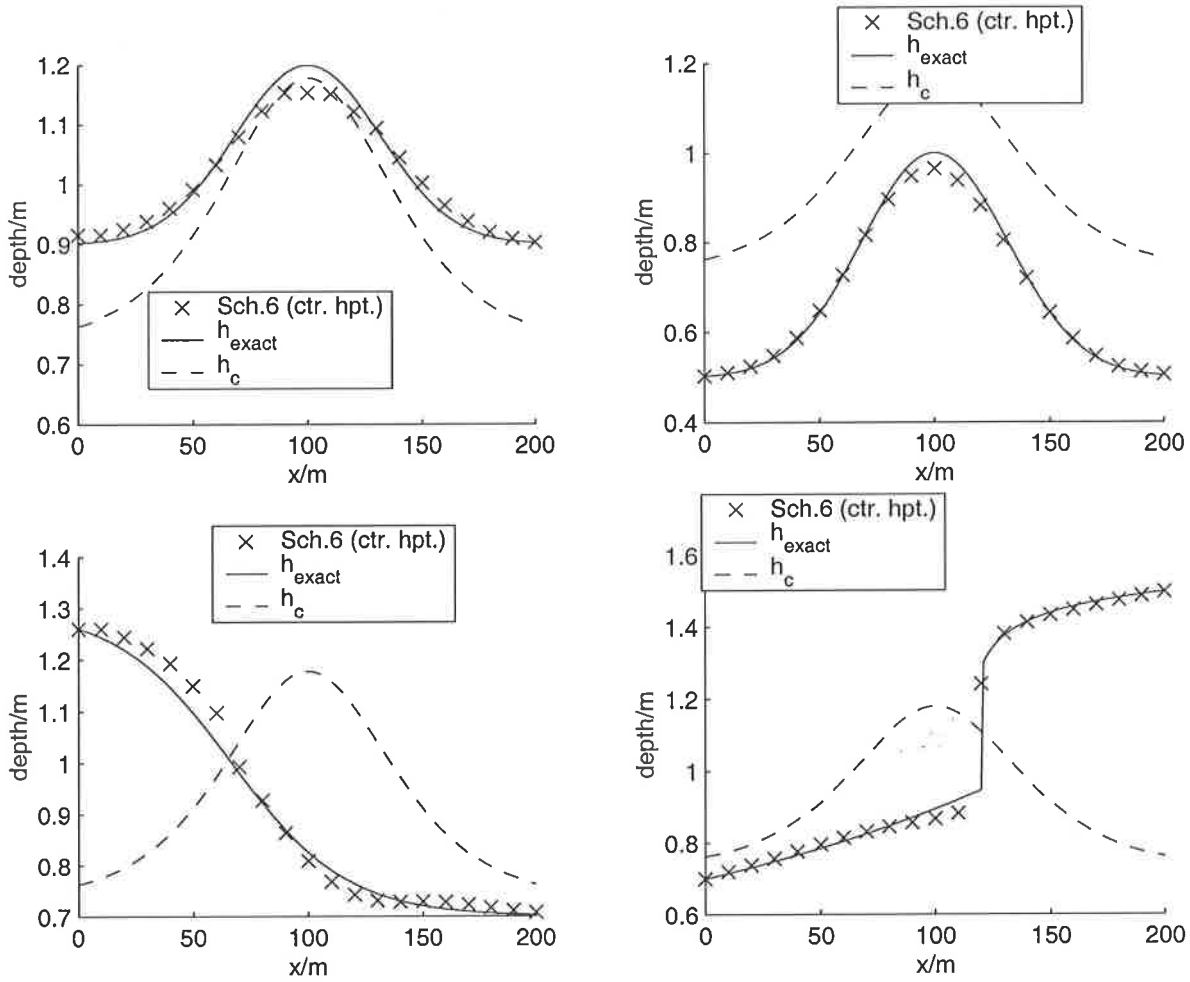

Figure 4.9: Scheme 6 (ctr. half-pt.) for problems 1-4 ($\Delta x = 10$)

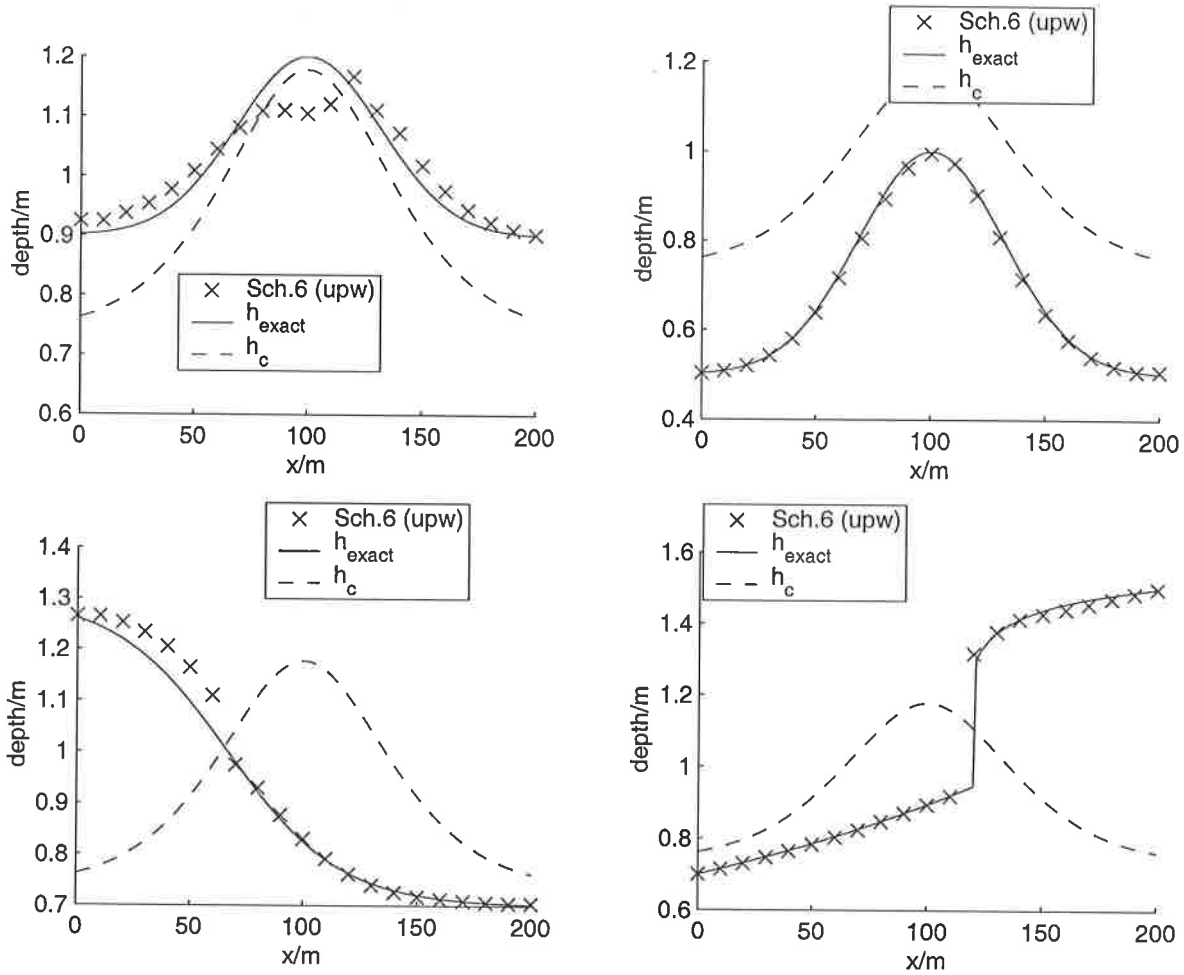

Figure 4.10: Scheme 6 (upw) for problems 1-4 ($\Delta x = 10$)

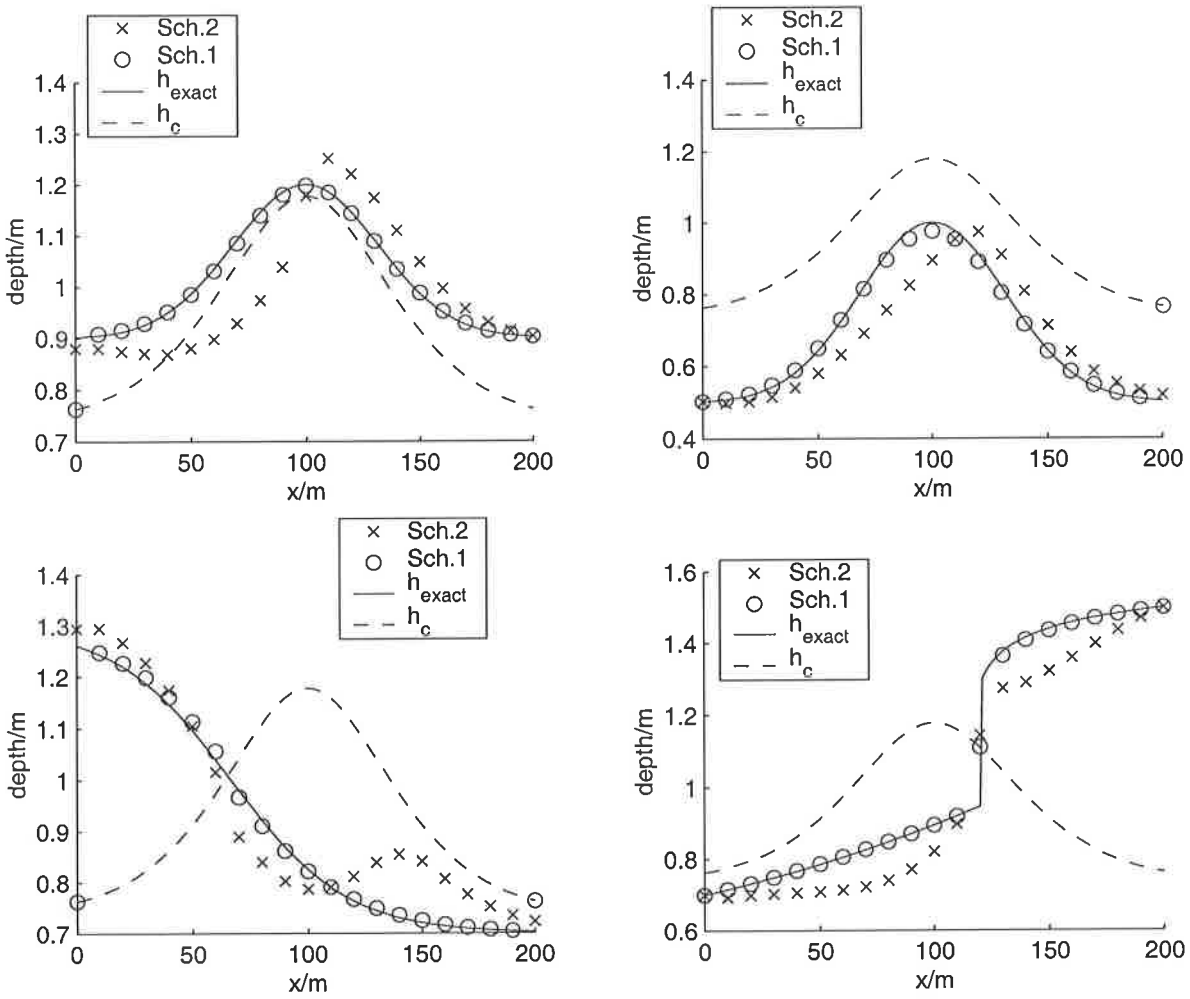

Figure 4.11: Schemes 2 and 1 for problems 1-4 ($\Delta x = 10$)

Comparing Engquist-Osher based schemes 1 (direct) and 5 (indirect) we can see (Fig. 4.12 or 4.21) that the approximate solution of scheme 1 is more accurate for test problems 1, 2 and 4 whereas the approximate solution of scheme 5 is more accurate for test problem 3. Neverthless, for test problem 4, the L_2 error is smaller in scheme 5 than in scheme 1 (see Figure 4.28).

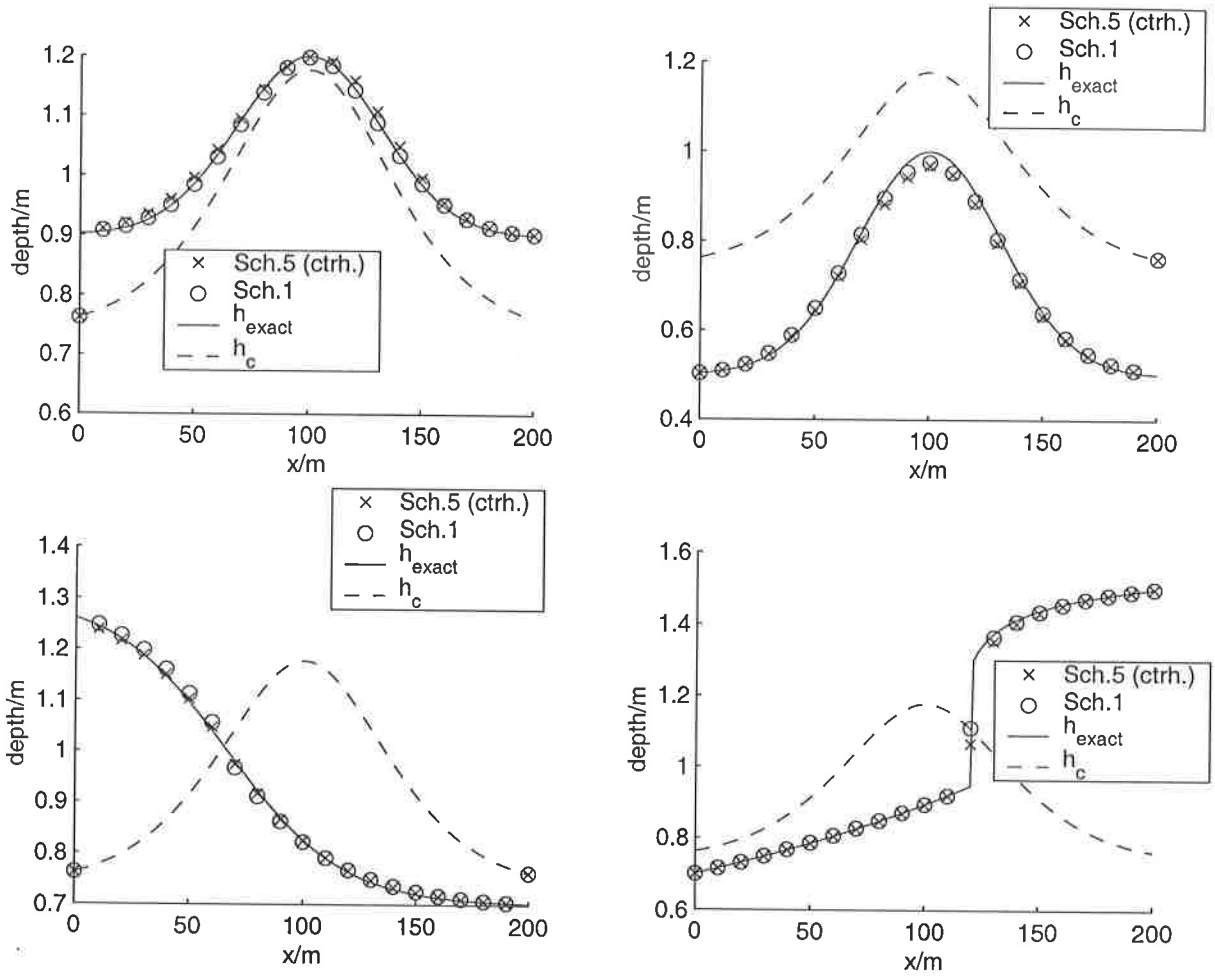

Figure 4.12: Schemes 5 (centred half-point) and 1 for problems 1-4 ($\Delta x = 10$)

Comparing Roe-based schemes 2 (direct) and 6 (indirect), we can see that the approximate solution obatined from scheme 6 is considerably more accurate than the approximate solution obtained from scheme 2, for all test problems (see Fig. 4.13).

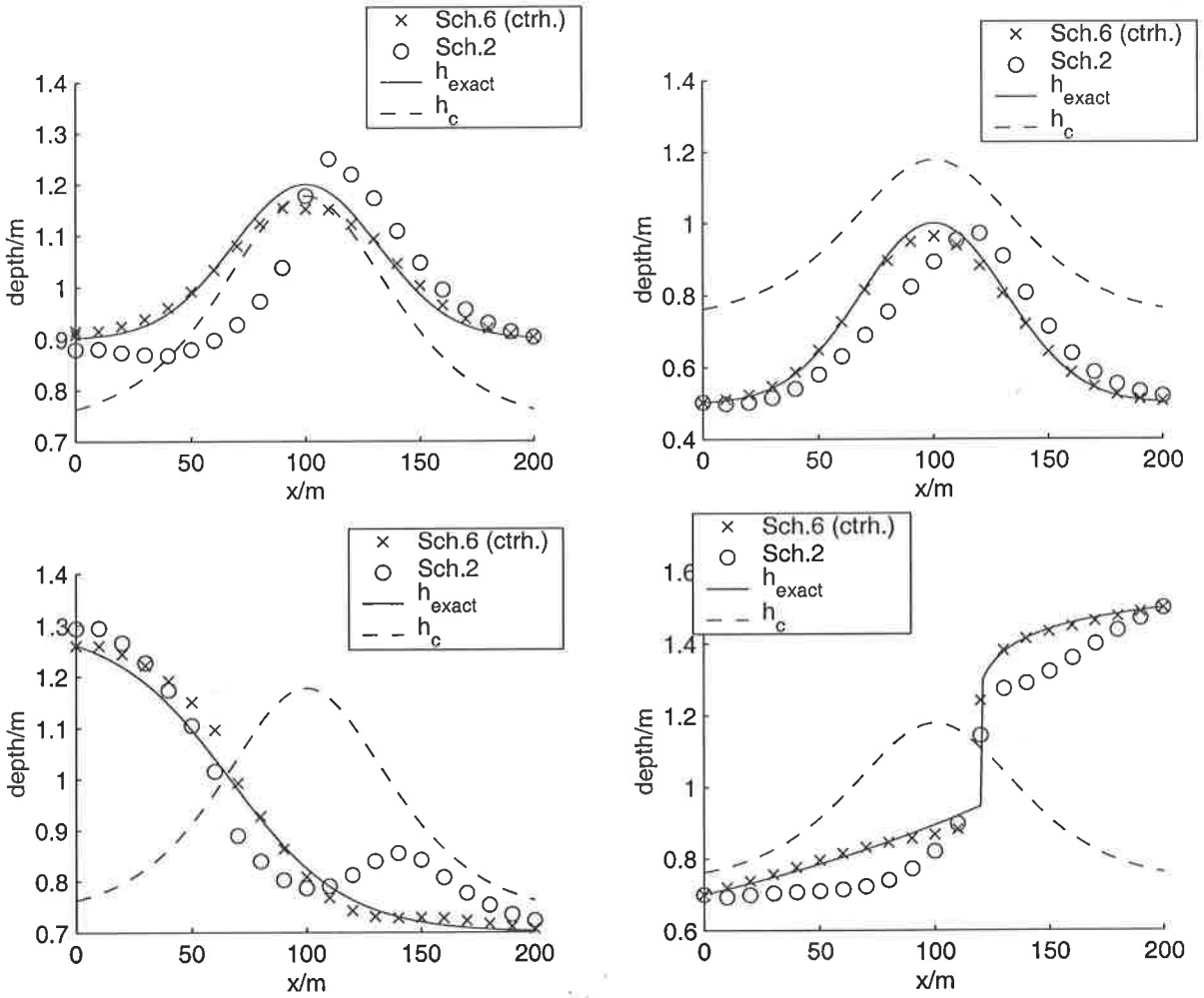

Figure 4.13: Schemes 6 (centred half-point) and 2 for problems 1-4 ($\Delta x = 10$)

The approximate solutions obtained from Engquist-Osher based schemes (schemes 1, 3 and 5) seem to show that either the direct or the indirect approach perform well and better, in general, than Roe-based schemes (see Figures 4.21-4.28). However, the direct approach gives a more accurate solution to test problems 1 (subcritical flow) and 2 (supercritical flow) whereas the indirect approach performs better for test problems 3 (smooth transition) and 4 (hydraulic jump).

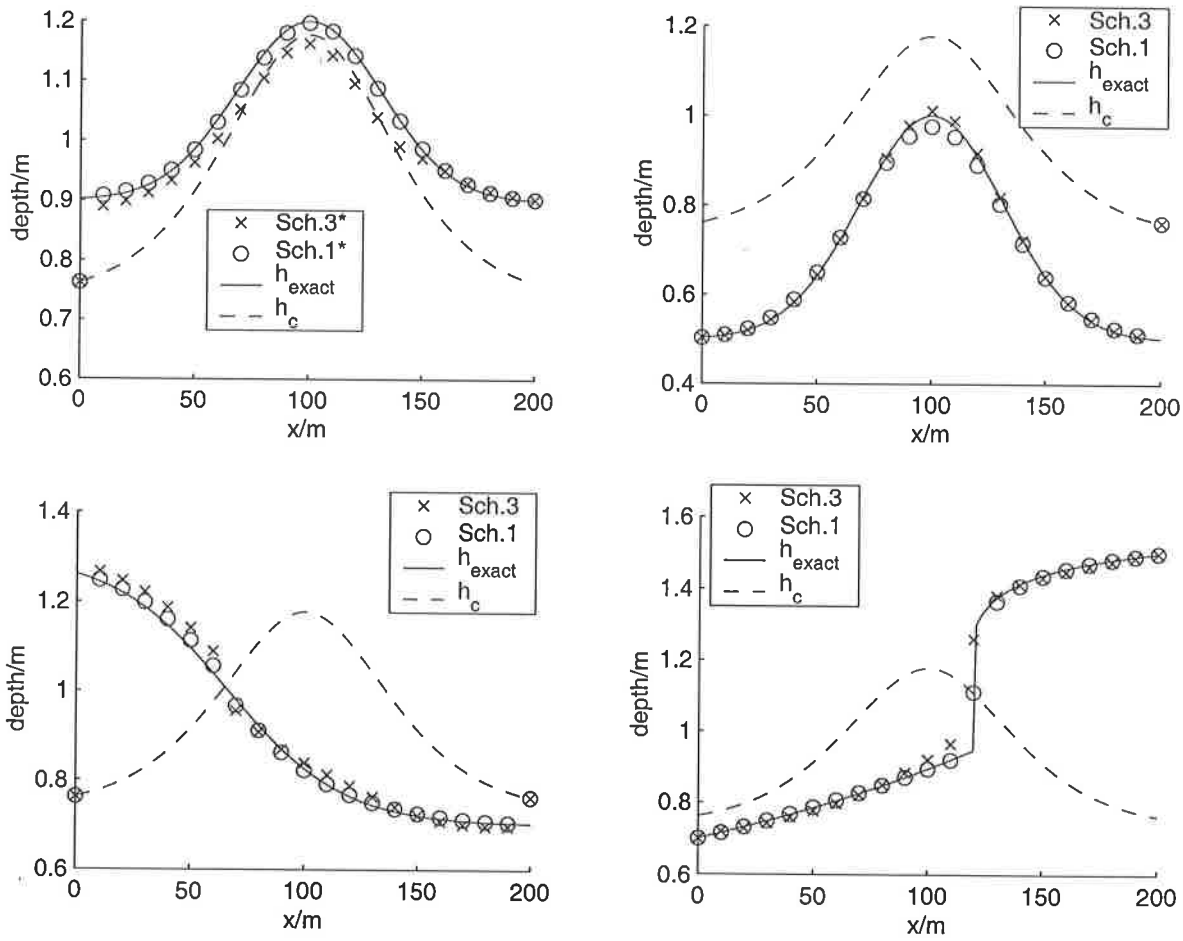

Figure 4.14: Scheme 3 and 1 for problems 1-4 ($\Delta x = 10$); '*' means that it was used TOL= 10^{-4}

In the indirect approach (schemes 5 and 6) the derivative put on the right-hand side was discretised in three diferent ways: centred discretised, centred discretised at the half-point and upwind discretised. The upwind discretisation implemented depends strongly on the computation of the critical depth function and on the critical x, which is relatively easy to compute for the case of rectangular cross-section but much more difficult for a more general prismatic cross-section. For the Roe-based schemes it seems easy to implement un upwind discretisation in the way Glaister [9] and others (e.g. [6, 2, 7]) have done. But an upwind discretisation of the right-hand side for Engquist-Osher based schemes has to be thought of. The numerical results for the different types of discretisation of the derivative on the right-hand side are shown in figures 4.15- 4.16. From the numerical results obtained, the centred approximation at the half-popint seems more accurate than the centred approximation for both schemes, 5 and 6 (remember that $D(x,h)$ is pointwise or averaged discretised in all the numerical results presented - see Section 3.3). In figures 4.18 and 4.19 we can compare the upwind discretisation and centred (half-point) discretisation of the right-hand side derivative for schemes 5 and 6.

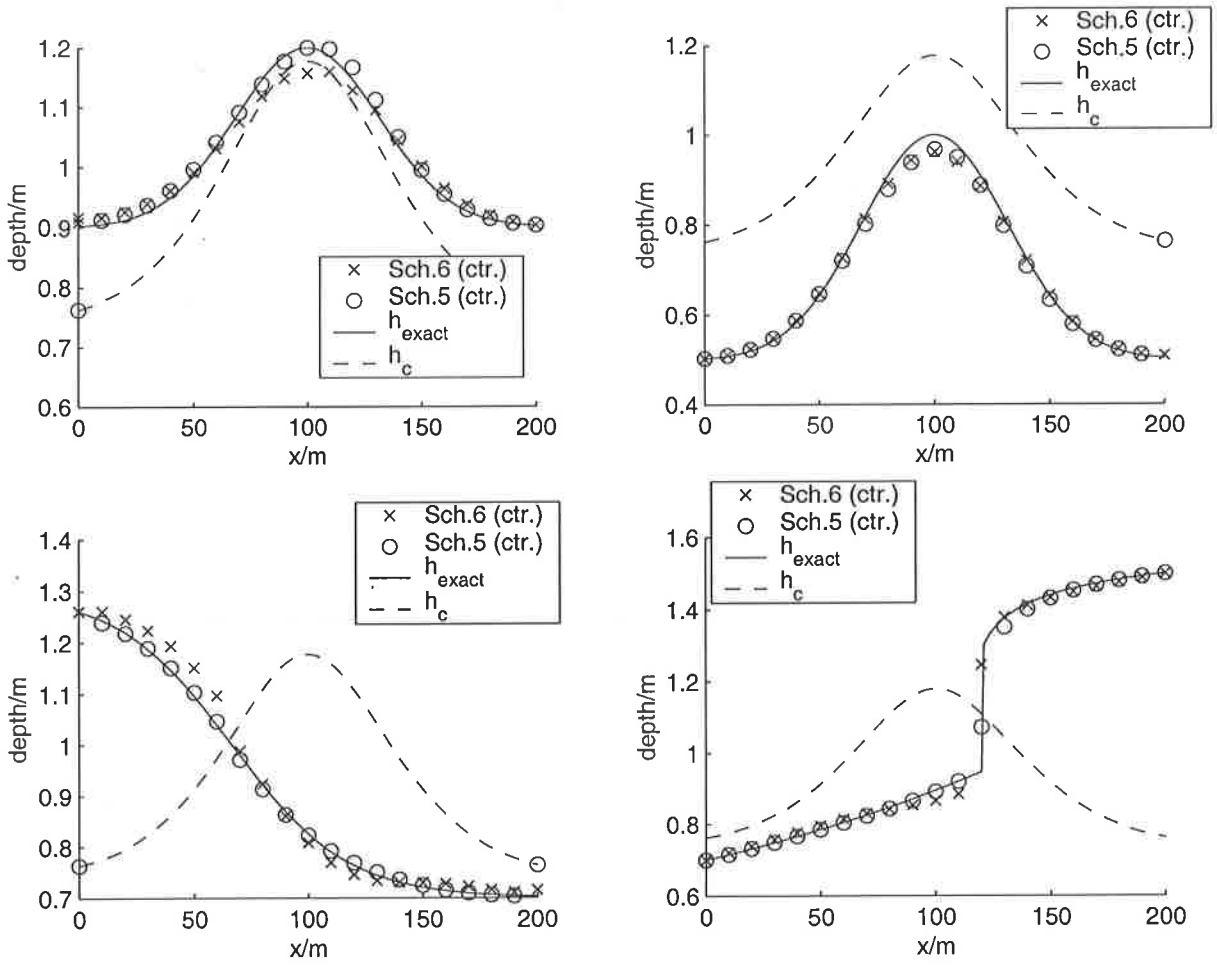

Figure 4.15: Schemes 6 and 5 (both centred) for problems 1-4 ($\Delta x = 10$)

The indirect approach of splitting the derivative and absorve $\frac{dF}{dx}$ in the source terms was the one followed in schemes 5 and 6 and as we can see from Figures 4.5-4.10 provides an accurate numerical solution. In almost all the test problems, scheme 5 is more accurate than scheme 6. The only exception is test problem 2 (see Figures 4.21, 4.23, 4.25 and 4.27)

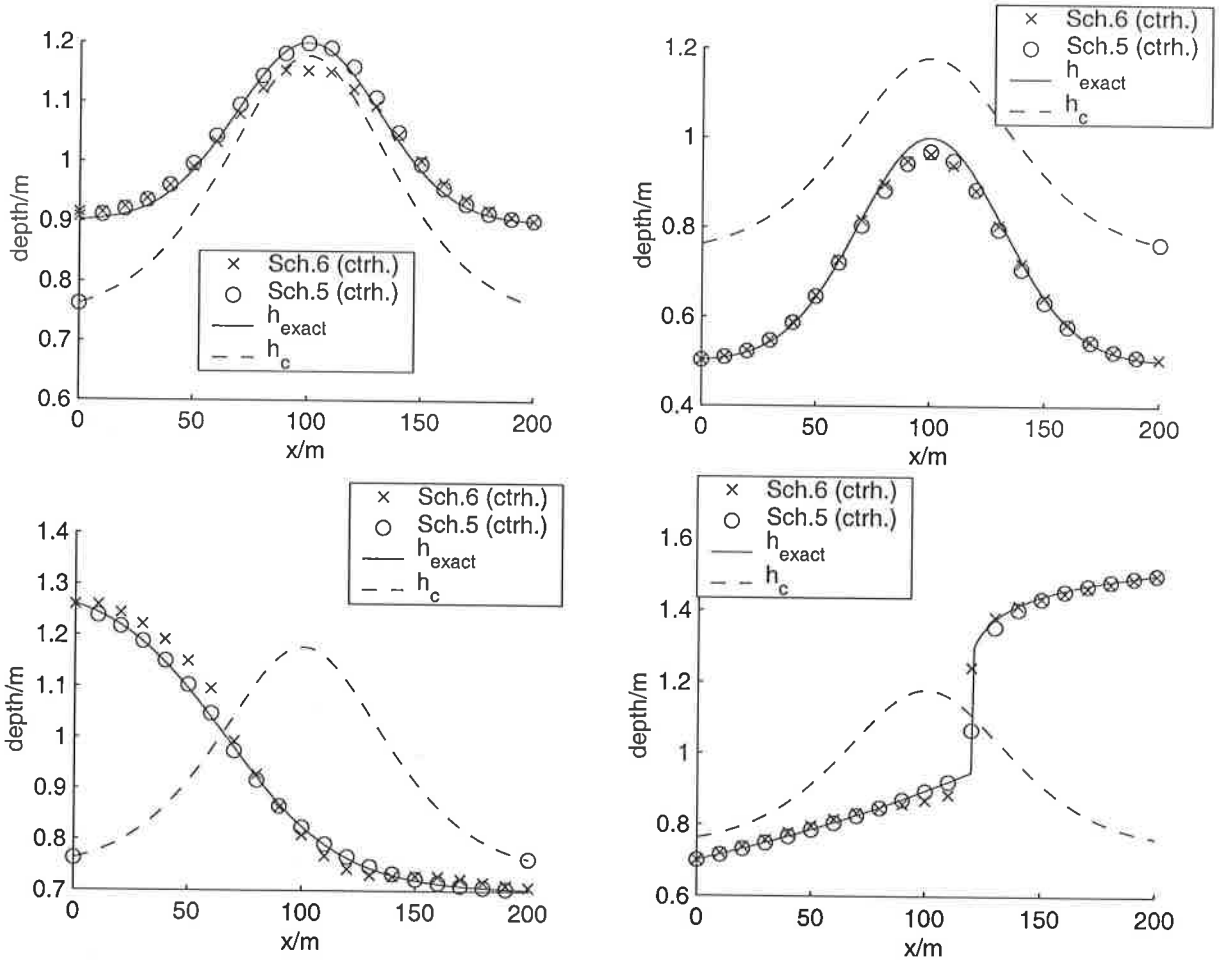

Figure 4.16: Schemes 6 and 5 (both half-point centred) for problems 1-4 ($\Delta x = 10$)

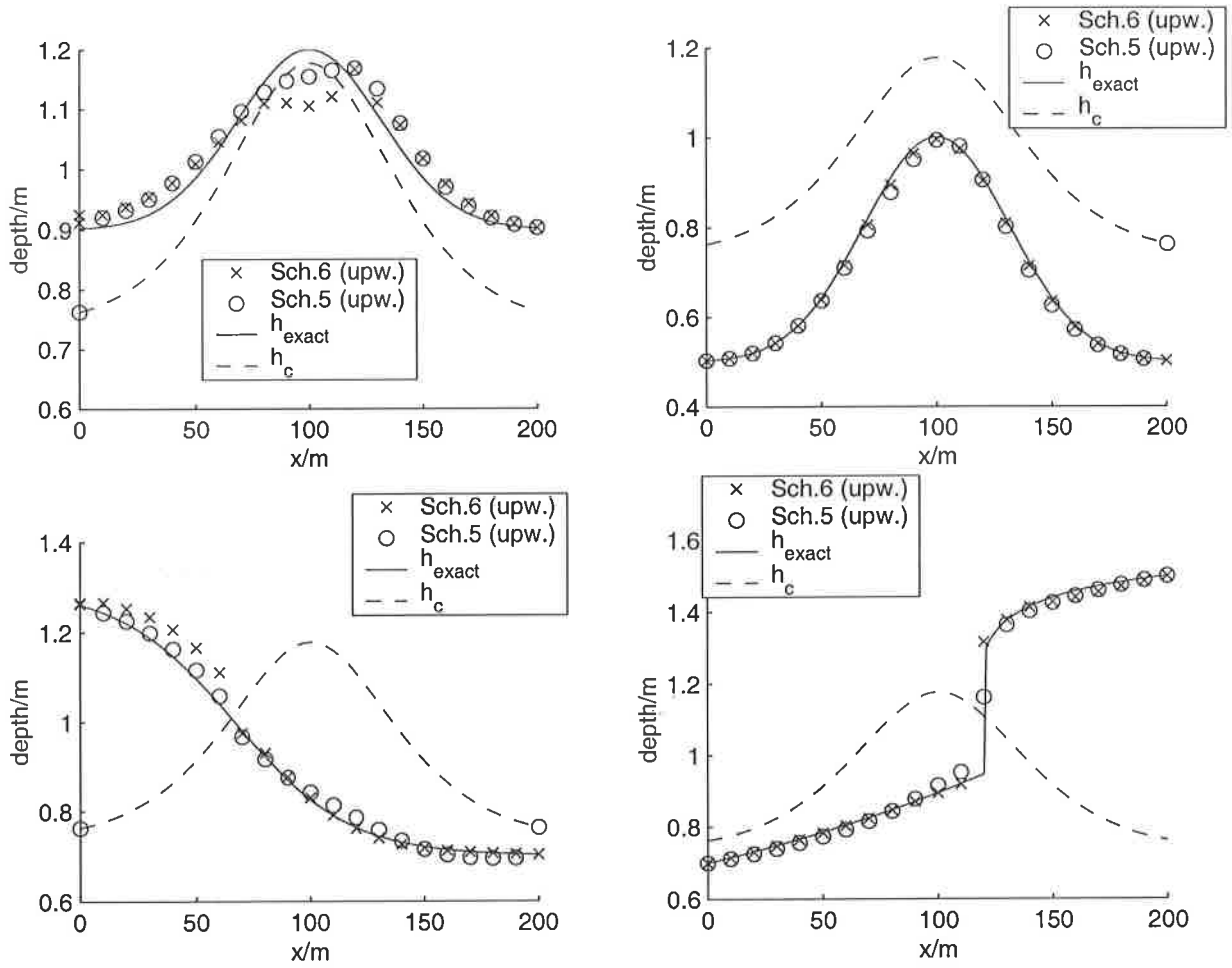

Figure 4.17: Schemes 6 and 5 (both upwind) for problems 1-4 ($\Delta x = 10$)

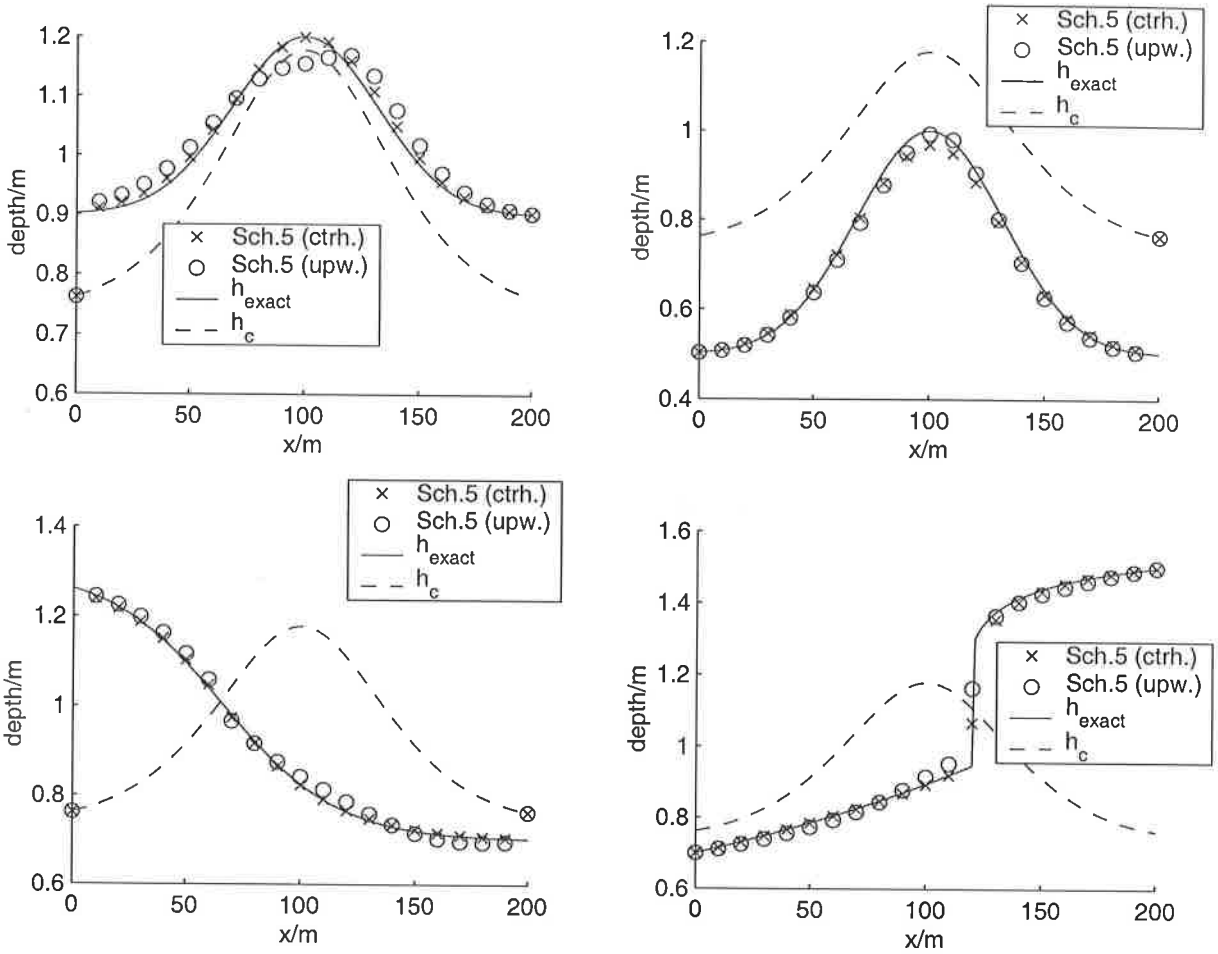

Figure 4.18: Scheme 5 (centred half-point and upwind) for problems 1-4 ($\Delta x = 10$)

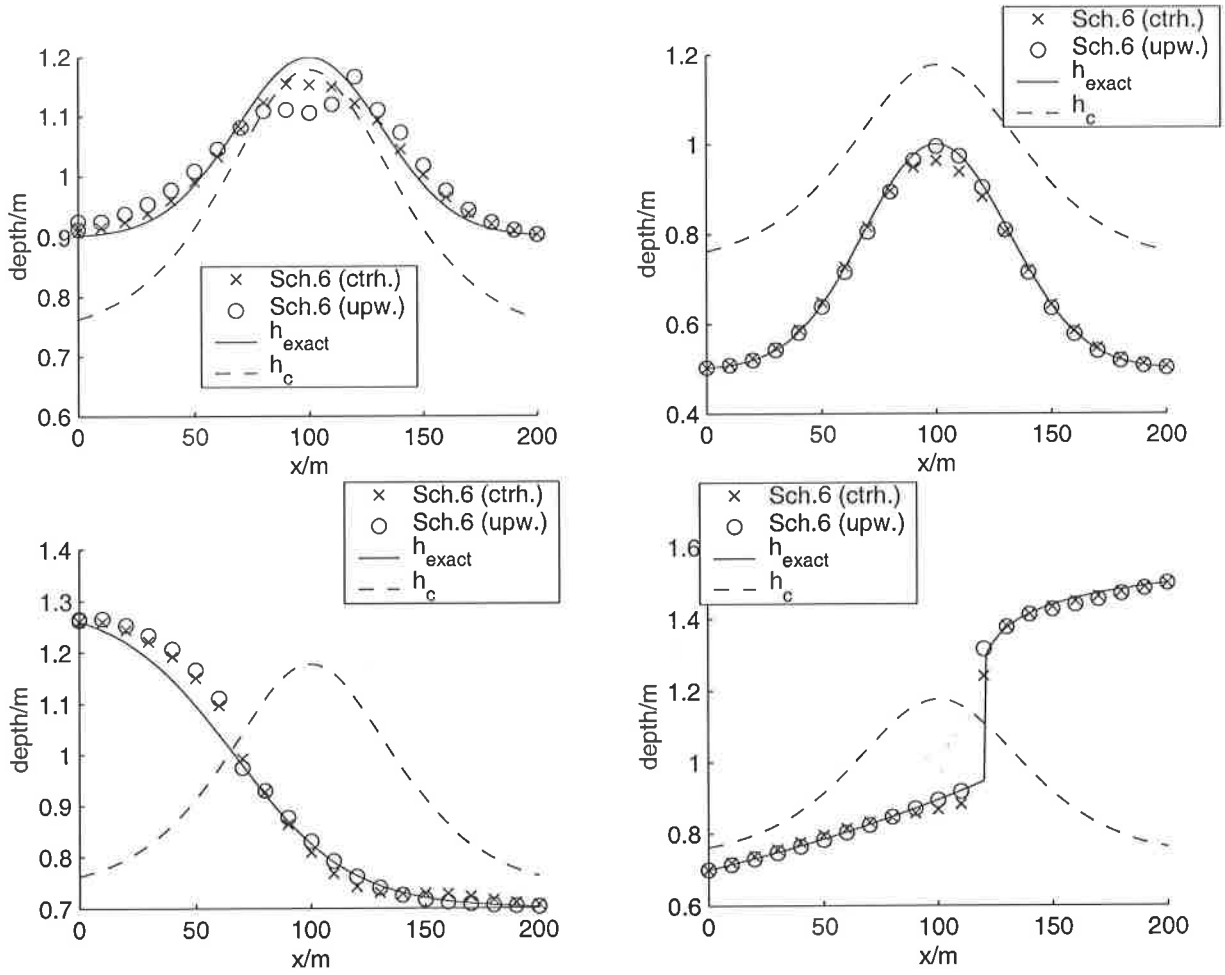

Figure 4.19: Scheme 6 (centred half-point and upwind) for problems 1-4 ($\Delta x = 10$)

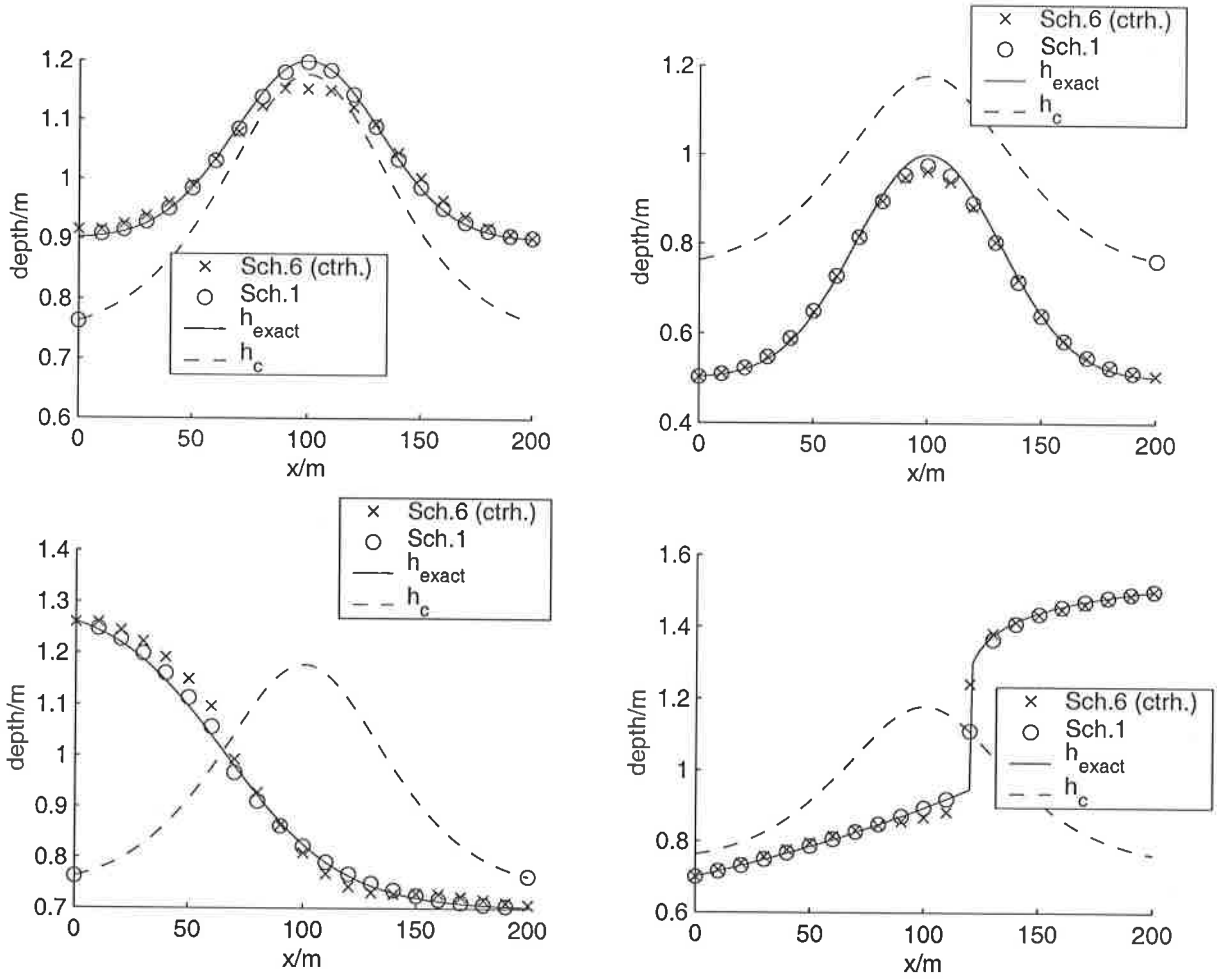

Figure 4.20: Schemes 6 (centred half-point) and 1 for problems 1-4 ($\Delta x = 10$)

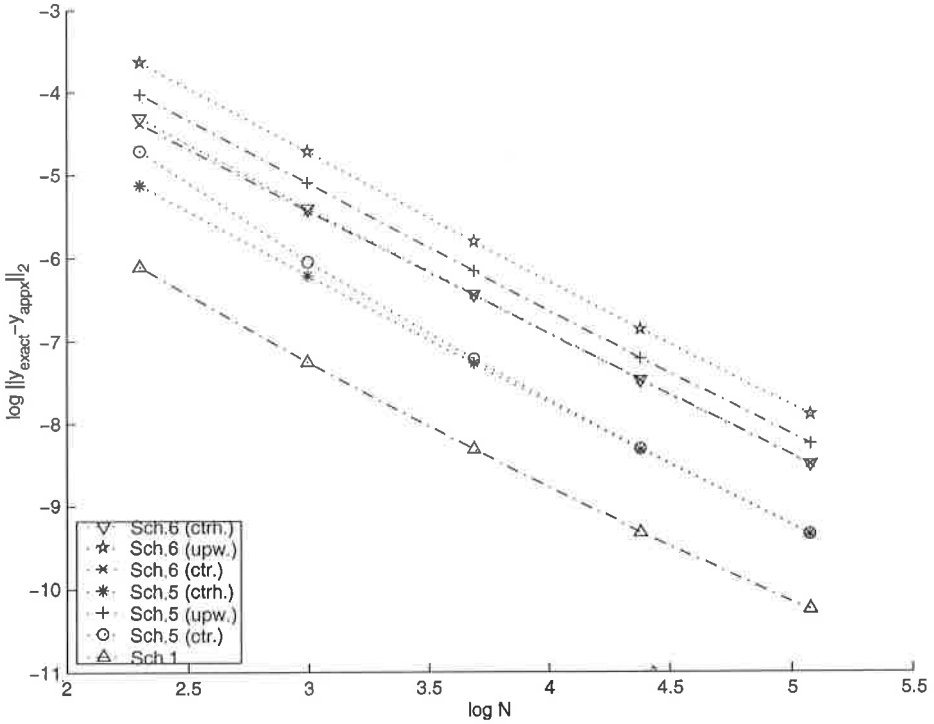

Figure 4.21: Schemes 6, 5 and 1 for test problem 1

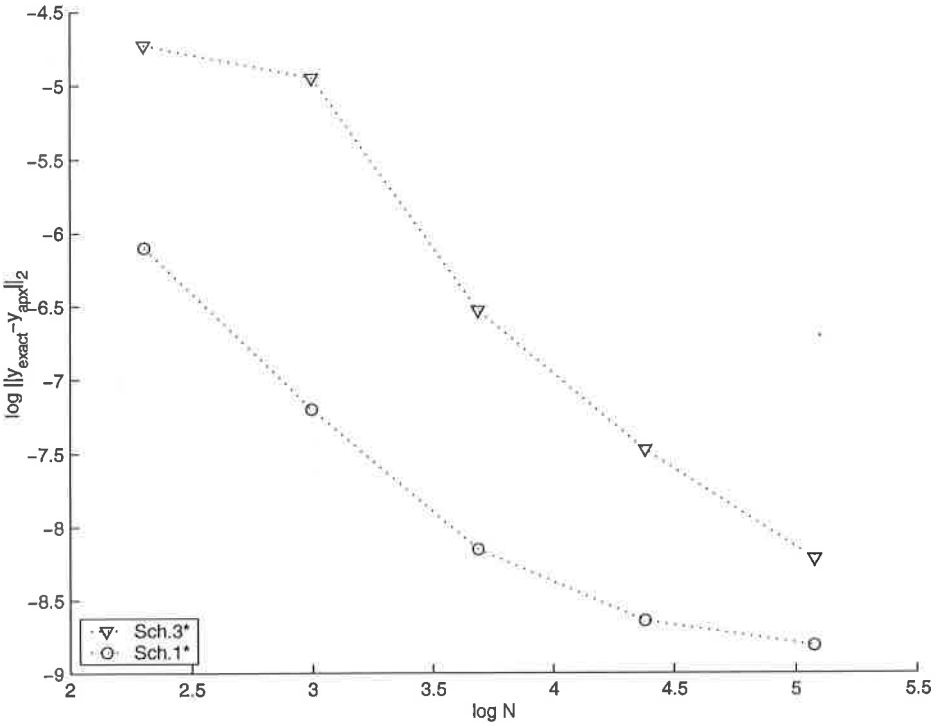

Figure 4.22: Schemes 3 and 1 for test problem 1 with $TOL = 10^{-4}$

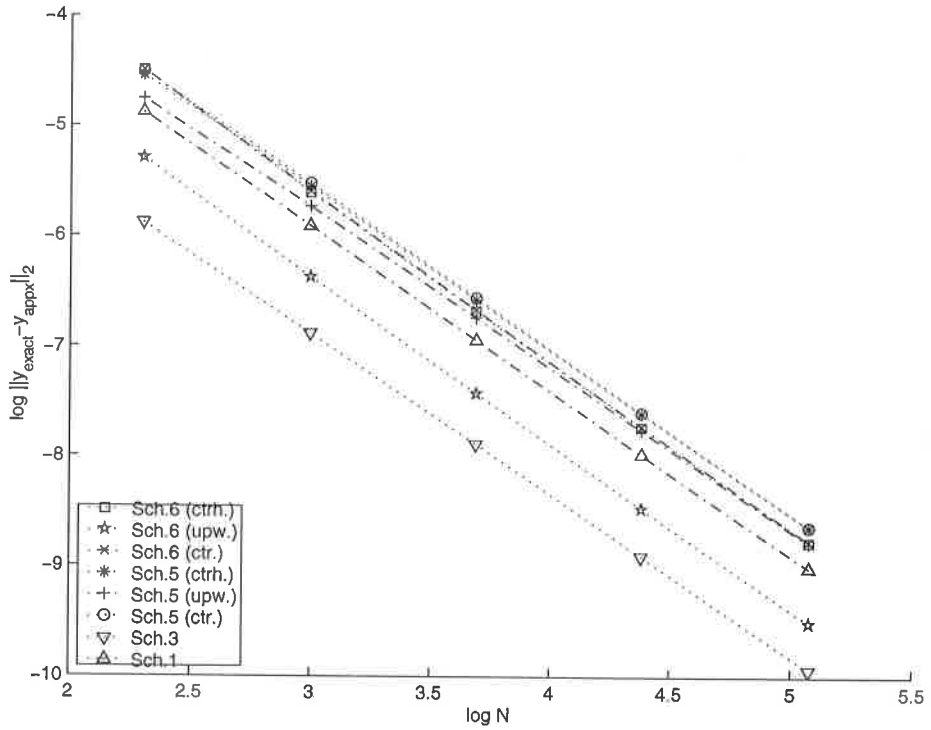

Figure 4.23: Schemes 6, 5, 3 and 1 for test problem 2

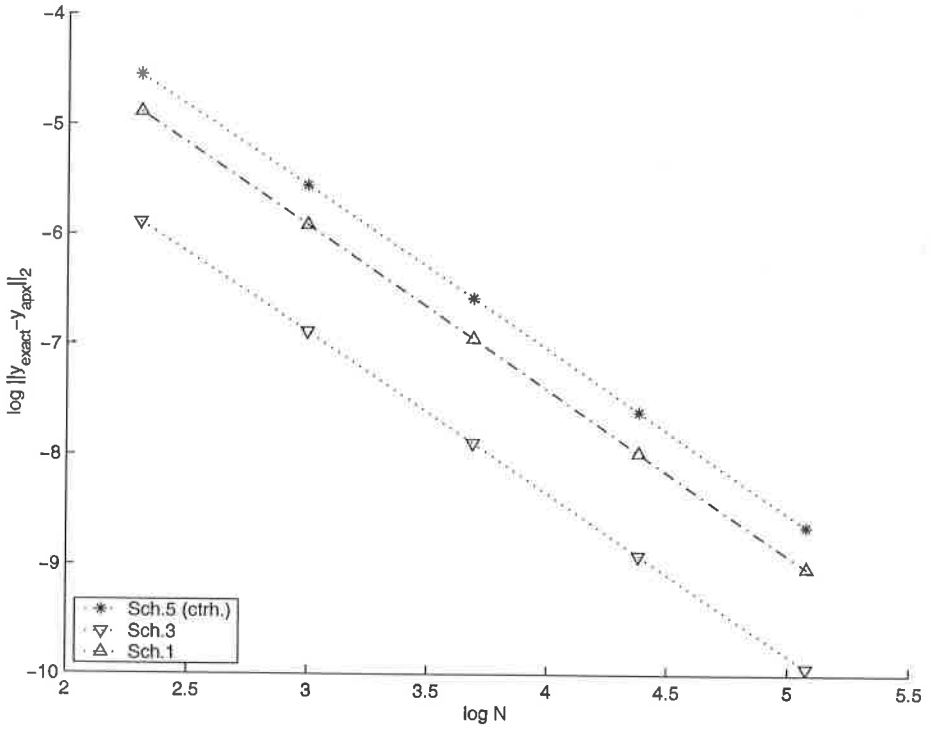

Figure 4.24: Schemes 5 (centred half-point), 3 and 1 for test problem 2

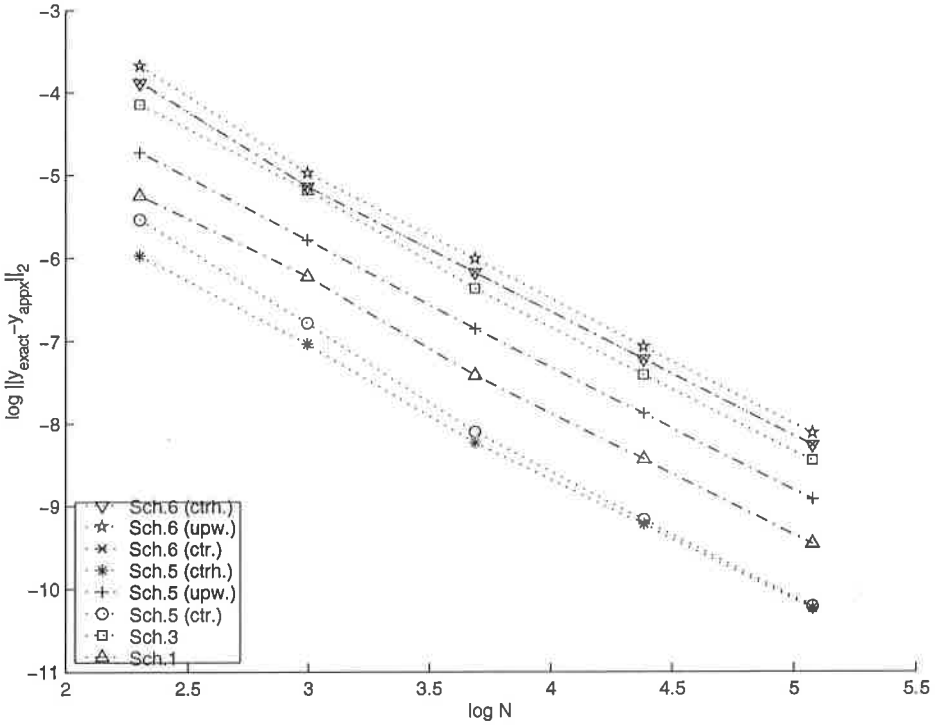

Figure 4.25: Schemes 6, 5, 3 and 1 for test problem 3

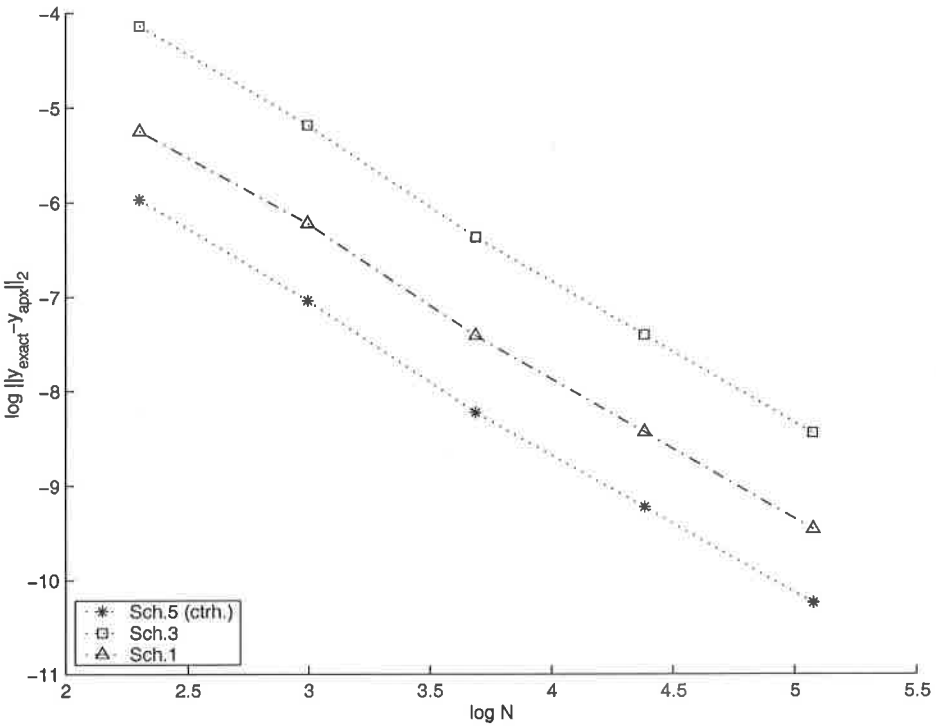

Figure 4.26: Schemes 5 (centred half-point), 3 and 1 for test problem 3

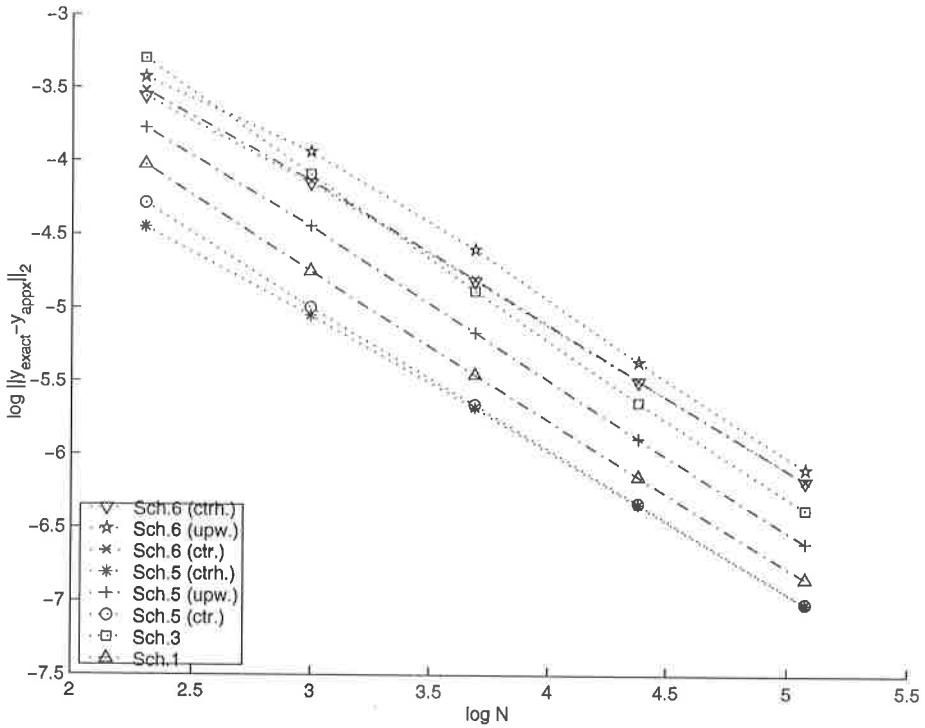

Figure 4.27: Schemes 6, 5, 3 and 1 for test problem 4

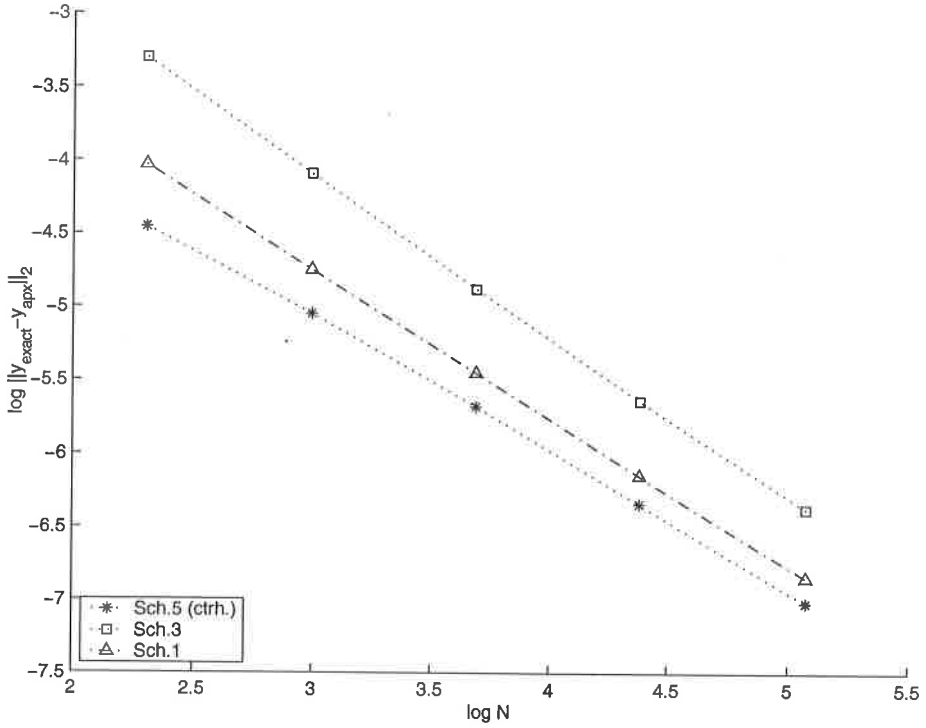

Figure 4.28: Schemes 5 (centred half-point), 3 and 1 for test problem 4

Chapter 5

Conclusions

In Section 4.2 the solutions to test problems 1-4 obtained by using schemes 1-3, 5-6 were presented and discussed. The test problems were chosen to represent different types of flow.

We have seen that the Engquist-Osher schemes (schemes 1, 3 and 5) provide a more accurate solution than the Roe schemes (with the type of source term discretisation studied here). The best Roe scheme is scheme 6 since scheme 4 does not converge and scheme 2 generates a solution that is not very accurate (see Figure 4.3). The work done by several authors (e.g. [2, 25, 13]) suggest that there should be a balance between the upwind discretisation of the flux functions, when using Roe scheme, and the discretisation of source terms. We intend to study our schemes in a similar manner in a next report.

For Roe schemes (schemes 2 and 6), the indirect approach provides a more accurate solution than the direct approach. The same is not true, in general, for Engquist-Osher schemes (schemes 1,3 and 5). We have seen that the direct approach generates a more accurate solution to test problems 1 and 2 (flow entirely subcritical or supercritical, respectively) whereas the indirect approach gives a more accurate solution to test problems 3 and 4 where there is a change in the flow (subcritical to supercritical and supercritical to subcritical, respectively).

In general, in the indirect schemes 5 and 6, the centred discretisation of the derivative on the right-hand side gives a more accurate approximation to the true (analytical) depth profile than the upwind discretisation. The only exception is test problem 2. Two ideas are worth studying. The first is whether this remains true even if $D(x,h)$ is also upwind discretised. The second idea is to modify the upwind approach implemented here since it is strongly dependent on the knowledge of the critical function h_c and follow the ideas in [13] or [2, 25] (and other authors) for Roe scheme. This latter idea means that the knowledge of the switch on the left-hand side given by the method adopted (Engquist-Osher-based or Roe-based) should be used to decide on the upwind of the source terms (combined or not with the upwind discretisation of $D(x,h)$ as well).

Bibliography

[1] J. D. Anderson, Jr. *Computational fluid Dynamics - the basics with applications.* McGraw-Hill International Editions, 1995.

[2] A. Bermudez and M. .E. Vazquez. Upwind methods for hyperbolic conservation laws with source terms. *Computers Fluids*, 8:1049–1071, 1994.

[3] V. T. Chow. *Open-Channel Hydraulics.* McGraw-Hill International Editions, 1959.

[4] S. Emmerson. *Modelling of Transient Dynamics of Gas Flow in Pipes.* PhD thesis, University of Reading, 1991.

[5] B. Engquist and S. Osher. One-sided difference approximations for nonlinear conservation laws. *Mathematics of Computation*, 36:321–351, 1981.

[6] P. Garcia-Navarro and M. E. Vazquez-Cendon. Some considerations and improvements on the performance of Roe's scheme for 1D irregular geometries. unpublished: prepublicacion Univ. Santiago de Compustela (given to me by Matthew Hubbard), 1997.

[7] P. Garcia-Navarro and M. E. Vazquez-Cendon. On numerical treatment of the source terms in the shallow water equations. *Computers and Fluids*, 29:951–979, 2000.

[8] P. Glaister. Flux difference splitting techniques for the Euler equations in non-cartesian geometry. Numerical Analysis Report 8/85, Department of Mathematics, University of Reading, 1985.

[9] P. Glaister. Difference schemes for the shallow water equations. Numerical Analysis Report 9/87, Department of Mathematics, University of Reading, 1987.

[10] P. Glaister. Prediction of supercritical flow in open channels. *Computers Math. Applic.*, 24:69–75, 1992.

[11] E. Godlewski and P.-A. Raviart. *Numerical approximation of hyperbolic systems of conservation laws.* Springer-Verlag, 1996.

[12] J. M. Greenberg and A. Y. Leroux. A well-balanced scheme for the numerical processing of source terms in hyperbolic equations. *SIAM Journal of Numerical Analysis*, 33:1–16, 1996.

[13] M. E. Hubbard and P. Garcia-Navarro. Flux difference splitting and the balancing of source terms and flux gradients. *Journal of Computational Physics*, 165:89–125, 2000.

[14] D. Kröner. *Numerical Schemes for Conservation Laws.* Wiley & Teubner, 1997.

[15] R. J. LeVeque. *Numerical Methods for Conservation Laws.* Birkhäuser, 1992.

[16] R. J. LeVeque. Balancing source terms and flux gradients in high-resolution Godunov methods: the quasi-steady wave-propagation algorithm. *Journal of Computational Physics*, 146:346–365, 1998.

[17] R. J. LeVeque and H. C. Yee. A study of numerical methods for hyperbolic conservation laws with stiff source terms. *Journal of Computational Physics*, 86:187–210, 1990.

[18] I. MacDonald. *Analysis and Computation of Steady Open Channel Flow.* PhD thesis, University of Reading, 1996.

[19] A. Priestley. Roe-type schemes for super-critical flows in rivers. Numerical Analysis Report 13/89, Department of Mathematics, University of Reading, 1989.

[20] P. L. Roe. Approximate Riemann solvers, parameter vectors, and difference schemes. *Journal of Computational Physics*, 43:357–372, 1981.

[21] P. L. Roe. Upwind differencing schemes for hyperbolic conservation laws with source terms. In C. Carasso, P.-A. Raviart, and D. Serre, editors, *Nonlinear hyperbolic problems.* Springer-Verlag, 1986.

[22] P. K. Sweby. Source terms and conservation laws: a preliminary discussion. Numerical Analysis Report 6/89, Department of Mathematics, University of Reading, 1989.

[23] P. K. Sweby. Godunov methods. Numerical Analysis Report 7/99, Department of Mathematics, University of Reading, 1999.

[24] E. F. Toro. *Riemann Solvers and Numerical Methods for Fluid Dynamics - a Practical Introduction.* Springer, 1999.

[25] M. E. Vázquez-Cendón. Improved treatment of source terms in upwind schemes for the shallow water equations in channels with irregular geometry. *Journal of Computational Physics*, 148:497–526, 1999.